

Targeting Gain of Function and Resistance Mutations in Abl and KIT by Hybrid Compound Design

André Richters,[†] Julia Ketzner,[‡] Matthäus Getlik,[†] Christian Grütter,[†] Ralf Schneider,[§] Johannes M. Heuckmann,[⊥] Stefanie Heynck,[⊥] Martin L. Sos,[⊥] Anu Gupta,[▽] Anke Unger,[#] Carsten Schultz-Fademrecht,[#] Roman K. Thomas,^{⊥||} Sebastian Bauer,^{‡,*} and Daniel Rauh^{†,§,*}

[†]Department of Chemistry and Chemical Biology, Technical University of Dortmund, Otto-Hahn-Strasse 6, D-44227 Dortmund, Germany

[‡]Department of Medical Oncology, Sarcoma Center, West German Cancer Center, University Duisburg-Essen Medical School, Hufelandstrasse 55, D-45122 Essen, Germany

[§]Chemical Genomics Centre of the Max-Planck-Society, Otto-Hahn-Strasse 15, D-44227 Dortmund, Germany

[⊥]Department of Translational Genomics, University of Cologne, Weyertal 115b, D-50931 Cologne, Germany

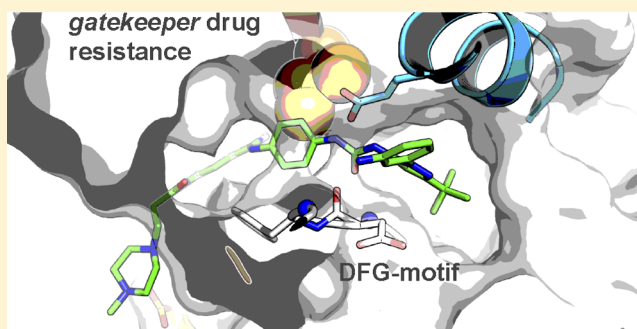
^{||}Department of Pathology, University of Cologne, Joseph-Stelzmann Strasse 9, D-50931 Cologne, Germany

[▽]Department of Molecular Genetics, Lerner Research Institute, Cleveland Clinic, Cleveland, Ohio 44195, United States

[#]Lead Discovery Center GmbH, Otto-Hahn-Strasse 15, D-44227 Dortmund, Germany

Supporting Information

ABSTRACT: Mutations in the catalytic domain at the gatekeeper position represent the most prominent drug-resistant variants of kinases and significantly impair the efficacy of targeted cancer therapies. Understanding the mechanisms of drug resistance at the molecular and atomic levels will aid in the design and development of inhibitors that have the potential to overcome these resistance mutations. Herein, by introducing adaptive elements into the inhibitor core structure, we undertake the structure-based development of type II hybrid inhibitors to overcome gatekeeper drug-resistant mutations in cSrc-T338M, as well as clinically relevant tyrosine kinase KIT-T670I and Abl-T315I variants, as essential targets in gastrointestinal stromal tumors (GISTs) and chronic myelogenous leukemia (CML). Using protein X-ray crystallography, we confirm the anticipated binding mode in cSrc, which proved to be essential for overcoming the respective resistances. More importantly, the novel compounds effectively inhibit clinically relevant gatekeeper mutants of KIT and Abl in biochemical and cellular studies.



■ INTRODUCTION

Protein kinases represent a major enzyme family comprised of more than 500 members encoded in the human genome, which are involved in several signal transduction processes, including those responsible for cell proliferation, apoptosis, and cell survival.^{1–3} Since deregulation of signaling pathways, especially by constitutive activation of kinases, often leads to the onset of various diseases, including cancer, the inhibition of kinases has been at the leading edge of cancer research for decades.⁴

Various kinase inhibitors bind to the ATP binding site (type I and II inhibitors)^{5–8} and have proven to be powerful tools in the treatment of cancer. Imatinib targets tyrosine kinases such as KIT in gastrointestinal stromal tumors (GISTs)^{9,10} and Bcr-Abl in chronic myelogenous leukemia (CML).¹¹ Similarly, gefitinib targets EGFR in non-small-cell lung cancer (NSCLC).¹² Although these inhibitors are very successful in early disease stages in selected patient populations, the emergence of drug resistance during later stages of treatment is becoming an ever-increasing challenge.¹³ DNA

sequencing efforts of primary tumors show a high incidence of mutations in the active site of targeted kinases, which are responsible for this resistance.¹⁴ Thus, drug resistance is a major problem in the long-term treatment with targeted cancer therapies.^{15–17} Treatment of CML patients with imatinib (Figure 1a), for instance, leads on average to the incidence of drug resistance mutations in the kinase domain of Bcr-Abl or intolerance to imatinib in 30% of examined patient populations in the first five years.¹³ Even more dramatically, in the case of patients suffering from solid GISTs, 14% of patients initially do not respond to imatinib treatment and 50% will develop resistance mutations in the kinase domain of the stem cell growth factor receptor KIT within the first two years.⁹ Likewise, the efficacy of gefitinib in the treatment of NSCLC is significantly impaired by acquired resistance mutation T790M at the gatekeeper position of EGFR and renders even second-generation inhibitors that

Received: March 19, 2013

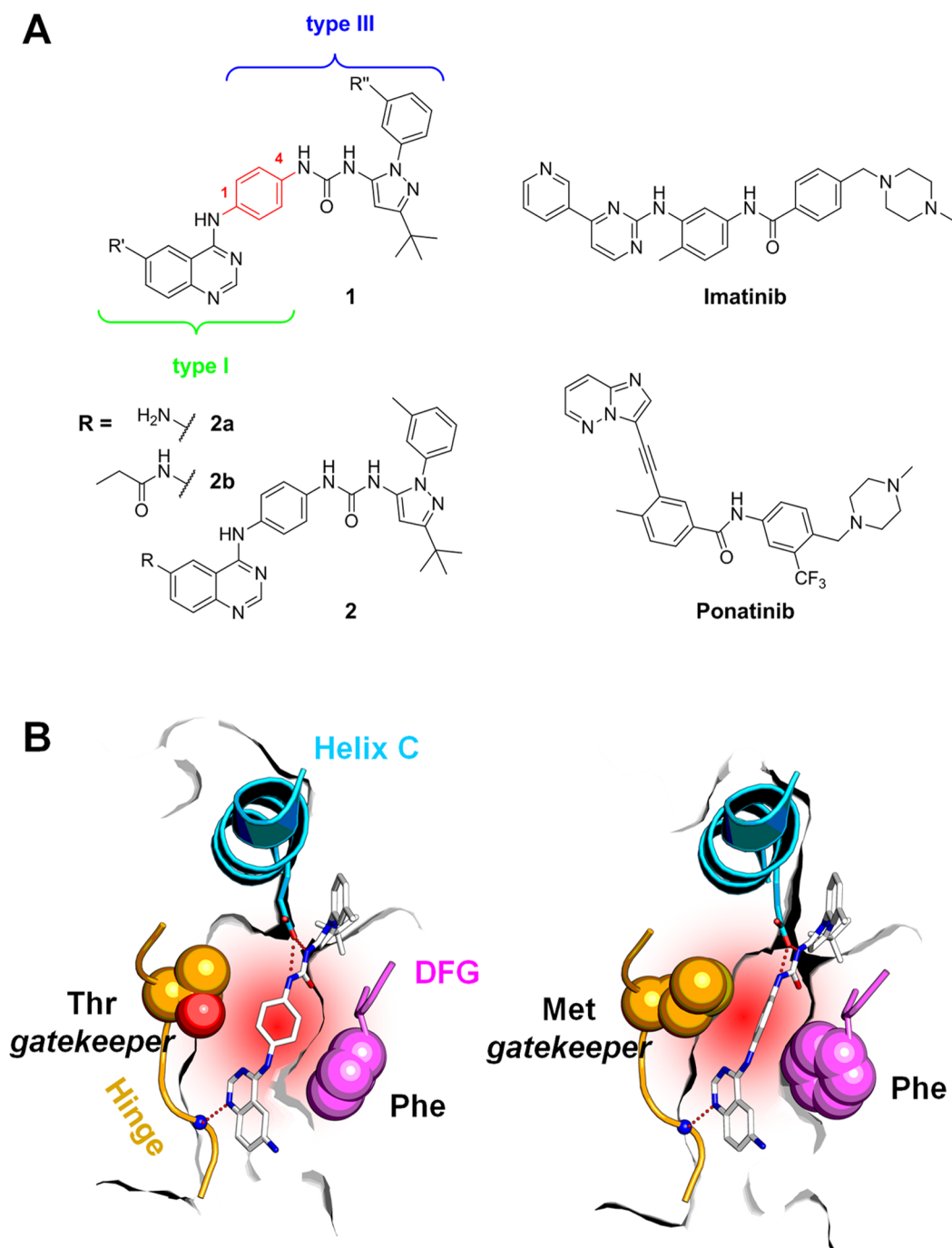


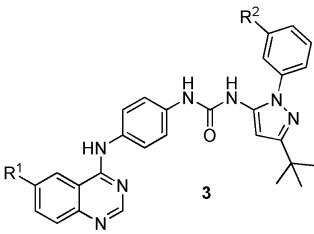
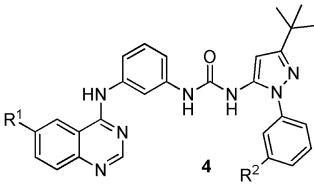
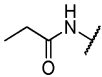
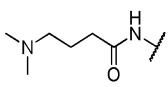
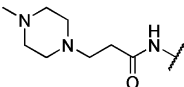
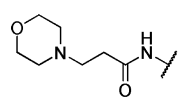
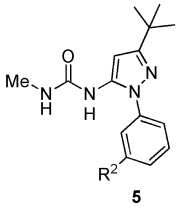
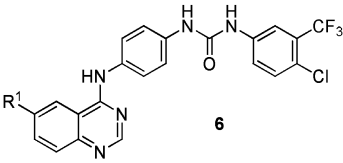
Figure 1. (A) General scaffold of a 1,4-fused type II hybrid inhibitor, **1**, composed of type I and type III fragments, as well as hybrid compound **2**, as an initial rationally designed molecule to target cSrc wild-type and T338M. Imatinib and ponatinib represent approved type II inhibitors for the treatment of GISTs and CML. (B) Schematic overview on how to circumvent steric repulsion with bulky gatekeepers (e.g., methionine) in drug-resistant mutant kinases.

irreversibly modify a rare cysteine at the lip of the catalytic cleft with only limited clinical impact.^{18,19} This demonstrates that the development of new and selective inhibitors that can inhibit clinically relevant kinases is still of major importance for the treatment of diseases such as GIST, CML, and NSCLC.

One of the most prominent and striking mutations is the replacement of the gatekeeper residue, a position that is known to control access to the ATP-binding site affecting inhibitor selectivity, with a bulkier and often more lipophilic residue, as is the case for T670I of the KIT oncogenic drug-resistant variant in GIST. The primary gain of function mutation V559D in the

juxtamembrane region of KIT leads to constitutive activation, while the secondary mutation T670I at the gatekeeper position is accompanied by insensitivity toward imatinib as a first line therapy.^{20,21} Similarly the oncogenic fusion protein Bcr-Abl in CML results in stabilization of the active kinase conformation leading to a constitutively active protein. Additionally, the amino acid exchange of threonine for isoleucine at the gatekeeper position 315 (T315I) causes a steric repulsion that prohibits inhibitors from binding within the active site and causes resistance to imatinib.²² Moreover, this substitution at position 315 represents the only variant out of more than

Table 1. Overview of Rationally Designed Small Molecule Library Consisting of Variably Fused 1,4- and 1,3-Fused Hybrid Derivatives as Well as Fragments and Compounds with Replaced Pyrazolo Part

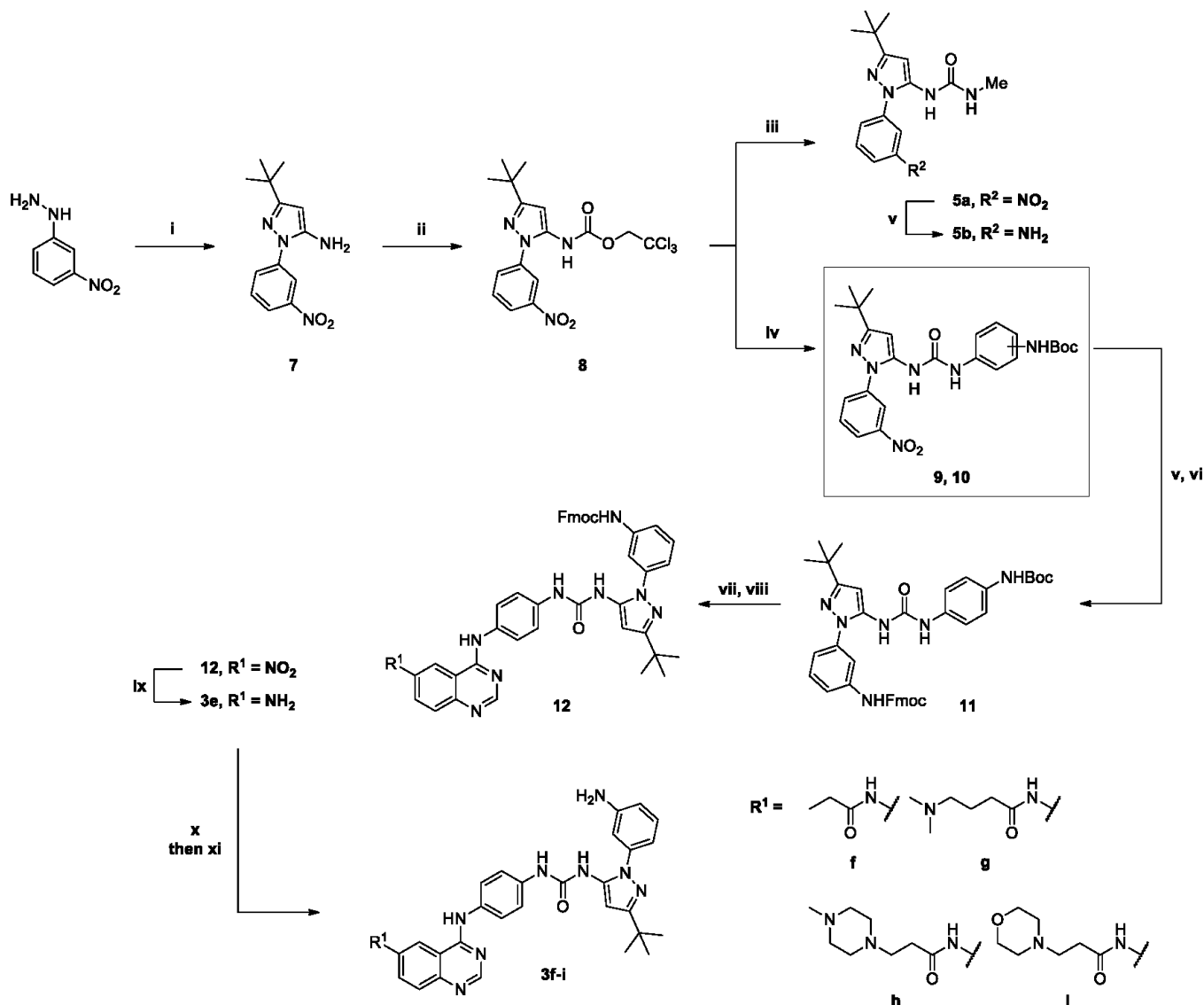
	Compound	R ¹	R ²
 3	3a	NO ₂	NO ₂
	3b	H	NO ₂
	3c	NH ₂	NH ₂
	3d	H	NH ₂
	3e	NH ₂	NHFmoc
 4	3f		NH ₂
	3g		NH ₂
	3h		NH ₂
	3i		NH ₂
 5	4a	H	NO ₂
	4b	H	NH ₂
 6	5a	---	NO ₂
	5b	---	NH ₂
	6a	NO ₂	---
	6b	NH ₂	---

50 drug-resistant mutations occurring in the catalytic domain of Bcr-Abl that is presently unfeasible to address in cancer therapy with small molecule inhibitors²³ with one exception: the type II inhibitor ponatinib (Figure 1a) recently received accelerated approval by the FDA while still running in phase III clinical trials, but treatment potentially produces severe side effects such as hepatotoxicity and arterial thrombosis.^{24,25} Therefore, current efforts in kinase research focus on overcoming these mutant variants by developing allosteric inhibitors that exclusively bind outside the ATP binding site and lock the kinase in its inactive form.^{26–29}

Recently, we presented the structure-guided development of type II inhibitors of cSrc. Fusion of a pyrazolo urea scaffold (type III, “allosteric”) with a quinazoline core (type I, ATP-competitive) resulted in potent type II cSrc inhibitors (1, Figure 1a) that lock the kinase in the inactive DFG-out conformation; these inhibitors were also active on the drug-resistant T338M gatekeeper mutant of cSrc. Protein X-ray crystallography revealed the rotational flexibility of a central 1,4-substituted phenyl ring of the inhibitor, which allows the hybrids to circumvent sterically demanding gatekeepers.³⁰ Here, we present the structure-guided optimization of those inhibitors to target the clinically relevant kinases KIT and Abl and their respective gatekeeper mutant forms T670I and T315I in biochemical and cellular systems.

RESULTS

Structure-Based Design of Type II Hybrid Inhibitors against cSrc, KIT, and Abl. Since cSrc, KIT, and Abl belong to closely related families of tyrosine kinases, we used the gatekeeper mutant cSrc T338M as an initial model system to transfer to KIT T670I and Abl T315I. To evaluate this, we generated a superimposed model of both (Figure S1, Supporting Information), based on the X-ray structure of cSrc T338M in complex with 2a (PDB 3F3W).³⁰ From this model, we predicted that a binding mode highly similar to cSrc would occur, suggesting that the new hybrid compounds would also show an inhibitory activity for KIT and Abl, as well as their gatekeeper mutant forms. The quinazoline N1 addresses the hinge, and the urea moiety is sandwiched between helix C and the DFG-motif of the kinase, which adopts its “out” conformation. A phenyl ring allowing for rotational flexibility links these parts of the inhibitor and interacts with the DFG-phenylalanine through a favorable edge-to-face orientation.³¹ The pyrazolo part points into the allosteric pocket, which is accessible only in the kinase’s inactive conformation.¹ Taking into account the hybrid compound’s ability to overcome gatekeeper mutations as for cSrc T338M, we proposed that these small molecules would be promising binders to inhibit the gatekeeper mutated forms of KIT T670I and Abl T315I.

Scheme 1. Synthesis of a Subset of Quinazoline Derivatives and Fragments^a

^aReagents and conditions: (i) Pivaloyl acetonitrile, conc. HCl, EtOH, 90 °C; (ii) Troc-Cl, NaOH, EtOAc/H₂O, 0 °C to rt; (iii) methylamine hydrochloride, DIPEA, DMSO, rt; (iv) *N*-Boc phenylenediamine, DIPEA, DMSO, rt; (v) ammonium formate, Pd/C, EtOH, 90 °C; (vi) Fmoc-Cl, NaHCO₃, dioxane/H₂O, rt; (vii) 4 M HCl in dioxane, rt; (viii) 4-chloro-6-aminoquinazoline, DIPEA, DCM, rt; (ix) iron chipping (activated with 1 N HCl), AcOH, EtOH, reflux; (x) corresponding acid chloride of **f-i**; THF, base (DIPEA or NMP), THF or DCM, rt; (xi) piperidine or morpholine in DMF, rt. The framed intermediate molecule was further used to generate other hybrid derivatives in a different synthetic route (See Supporting Information, Schemes S1 and S2).

Our optimization efforts were directed toward the extension of the hybrids at the quinazoline's 6-position with H-bond acceptor moieties (e.g., **3g,h**, Table 1). We speculated that introduction of polar motifs would lead to the formation of an additional contact at the lip of the active site to Asp348 in cSrc (data not shown), as well as to the corresponding residues Asn680 in KIT and Asp325 in Abl as shown in the case of **3g** (Figure S1, Supporting Information). In addition, the moderate solubility of the original compound would be increased. Furthermore, we exchanged the *meta*-positioned methyl group of the pyrazole connected phenyl ring with an amino moiety to improve the interaction within a polar subgroove adjacent to the allosteric binding site, which is formed by the polar side chain residues Glu310 (helix C), Asp404 (activation loop), and catalytic Lys295. We assumed that the ligand's polar interplay with this region would give further benefit to the affinity of these

hybrid compounds toward gatekeeper mutant forms of cSrc (T338M), KIT (T670I), and Abl (T315I). We also replaced the pyrazolo part by a 4-chloro-3-trifluoromethylphenyl moiety (**6**), the hydrophobic motif of the known multikinase inhibitor sorafenib,³² to study structure–activity relationships (SARs) among different implemented type III scaffolds and to achieve further increases in potency (Table 1).

Synthesis of a Focused Library of Hybrid Compounds and Fragments. We synthesized a focused library of variably fused type II inhibitors (Table 1) and paid particular attention to the derivatization of the quinazoline 6-position with various polar moieties frequently utilized in kinase inhibitor research (e.g., morpholine or methyl-piperazine).^{33,34} Since they exhibited different structural compositions, we expected these inhibitors to show a distinct SAR regarding their potency toward the investigated kinases. We especially expected the

Table 2. IC₅₀ Determinations of Hybrid Compounds and Fragments on Different Target Kinases

compd	IC ₅₀ (nM)					
	cSrc ^{WT}	cSrc ^{T338M}	Abl ^{WT}	Abl ^{T315I}	cKIT ^{WT}	cKIT ^{V559D/T670I}
3a	34.2 ± 22.6	126 ± 82.0	157 ± 76	561 ± 222	69.3 ± 19.3	637 ± 91
3b	19.9 ± 11.5	33.0 ± 5.1	42 ± 23	355 ± 116	7.3 ± 5.4	38.0 ± 16.4
3c	12.0 ± 0.5	5.9 ± 3.7	73 ± 36	81 ± 23	6.1 ± 1.9	7.6 ± 3.8
3d	37.9 ± 11.8	33.3 ± 10.2	40 ± 20	120 ± 43	3.3 ± 2.2	24.0 ± 3.7
3e	145 ± 47	211 ± 120	1273 ± 301	3620 ± 1180	20.9 ± 6.5	305 ± 69
3f	1.2 ± 0.5	1.7 ± 1.6	112 ± 45	441 ± 124	7.6 ± 1.6	22.1 ± 13.3
3g	1.1 ± 0.6	1.3 ± 0.2	124 ± 54	1170 ± 450	2.6 ± 0.5	2.7 ± 1.7
3h	1.1 ± 0.7	0.9 ± 0.4	61 ± 53	176 ± 47	3.5 ± 1.9	6.9 ± 2.7
3i	4.7 ± 2.1	3.5 ± 1.5	379 ± 70	820 ± 304	5.7 ± 3.4	9.2 ± 3.7
4a	39.3 ± 6.1	<i>a</i>	9 ± 7	<i>a</i>	29.2 ± 21.0	<i>a</i>
4b	304 ± 94	<i>a</i>	23 ± 4	<i>a</i>	30.1 ± 22.0	<i>a</i>
5a	<i>a</i>	<i>a</i>	<i>a</i>	<i>a</i>	<i>a</i>	<i>a</i>
5b	<i>a</i>	<i>a</i>	<i>a</i>	<i>a</i>	<i>a</i>	<i>a</i>
6a	<i>a</i>	<i>a</i>	<i>a</i>	<i>a</i>	4.5 ± 2.2	<i>a</i>
6b	3037 ± 200	<i>a</i>	<i>a</i>	<i>a</i>	1.0 ± 0.4	923 ± 305
2b	14 ± 1	23 ± 4	388 ± 88	141 ± 50	21.9 ± 6.1	155 ± 84
imatinib	2784 ± 481	<i>a</i>	19.9 ± 2.7	<i>a</i>	21.6 ± 7.0	≥100000
sunitinib	555 ± 48	134 ± 41	1613 ± 938	504 ± 102	0.7 ± 0.3	264 ± 92
ponatinib	0.9 ± 0.3	156 ± 27	2.9 ± 1.2	1.0 ± 0.5	1.7 ± 0.2	4.9 ± 0.6
dovitinib	80.8 ± 35.1	50.1 ± 15.4	450 ± 65	228 ± 67	1.1 ± 0.3	48.3 ± 5.2

^aNo inhibition at 100 μM compound concentration.

1,4-fused hybrids to perturb gatekeeper mutated forms of the kinases. The panel of inhibitors also included scaffolds with the pyrazolo part removed (**6a,b**) to (a) study the relevance of this structural motif concerning the binding affinity of the hybrid compounds and (b) further improve the inhibitory activity. Additionally, we incorporated type III pyrazolo-urea inhibitors (**5a,b**) into the set of tested compounds.

Hybrid compounds with different variations on the quinazoline 6-position were synthesized using a generic route (Scheme 1) starting with a Pinner-like cyclization of *m*-nitrophenyl hydrazine and pivaloyl acetonitrile to generate pyrazole **7**. The primary amine of **7** was then protected with 2,2,2-trichloroethyl chloroformate (Troc), yielding carbamate **8**, which subsequently was reacted with various primary amines to create the central urea moiety.³⁰ Fragments **5a** and **5b** were generated by treatment of **8** with methylamine hydrochloride to build up **5a**, and successive reduction with Pd/C provided the corresponding amine **5b**. Intermediates **9** and **10** were synthesized by reacting single Boc-protected 1,3- and 1,4-phenylenediamines with **8**. The 1,4-fused precursor **9** was then used to assemble quinazoline-pyrazoloureas **3e–i** by initial reduction to an intermediary amine and successive introduction of the orthogonal Fmoc-protecting group, providing **11**. An orthogonal protecting group strategy was essential to ensure selective derivatization of the quinazoline 6-position in **3e**. Next, 6-nitro-4-chloro-quinazoline was added via a two-step process, starting with Boc-deprotection and subsequent coupling of the quinazoline to form **12** by nucleophilic aromatic substitution (S_NAr). Reduction with Fe/AcOH provided **3e** which was further derivatized through direct amide formation with (*in situ* prepared) acid chlorides. Finally, Fmoc-cleavage provided compounds **3f–i**.

Quinazoline derivatives **3a**, **3b**, and **4a** were prepared via Boc-deprotection of intermediates **9** and **10** (see above). The corresponding amines **13** and **14** (Scheme S1, Supporting Information) were reacted with 6-nitro-4-chloroquinazoline or 4-chloroquinazoline, respectively, resulting in compounds **3a**,

3b, and **4a**. Reduction with Pd/C (for **3a**) or SnCl₂ (for **3b**, **4a**) to the corresponding amines **3c**, **3d**, and **4b** was conducted to complete this subset of derivatives.

Compounds **6a** and **6b** (Scheme S2) were made by initial reaction of 1-chloro-4-isocyanato-2-(trifluoromethyl)benzene with *tert*-butyl 4-aminophenylcarbamate. Boc-cleavage led to **15**, which then was treated with 4-chloro-6-nitroquinazoline to generate quinazoline urea **6a** in a S_NAr reaction. Finally, reduction with SnCl₂ was performed to prepare amine **6b**. Detailed synthetic procedures are described in the Experimental Section and Supporting Information.

Activity-Based *in Vitro* Characterization of Hybrid Compounds against cSrc. We characterized the focused compound collection against cSrc using an activity-based assay that quantifies phosphorylation of an artificial substrate by a particular kinase through homogeneous time-resolved FRET measurements (see Experimental Section). The observed IC₅₀ values (Table 2) confirmed an improved activity of the 1,4-fused hybrid compounds **3f–h** (~1 nM) with respect to both cSrc wild-type and its T338M mutant. In comparison to the most potent first generation hybrid compound (**2b**), this corresponded to a 14- and 23-fold increase in potency against wild-type and mutant cSrc, respectively. Converting the pyrazolo group into a 4-chloro-3-trifluoromethylphenyl moiety significantly decreased the affinity (**6a,b**) and demonstrated that the pyrazolo part is an important structural feature for preserving the binding affinity of the hybrids within the allosteric site of cSrc (Table 2). However, this element on its own (**5a,b**) did not show any inhibitory activity toward the protein due to the absence of the ability to lock the kinase in its inactive DFG-out conformation. Moreover, we illustrated a clear SAR among different derivatives concerning their efficacy against both cSrc variants. In general, the 1,4-fused hybrids **3f–h** were equally potent against both the wild-type and mutant kinase, while 1,3-fused analogs (**4a,b**) completely lost their potency against the mutant cSrc carrying the bulky methionine gatekeeper. This was to be expected from our previous study,

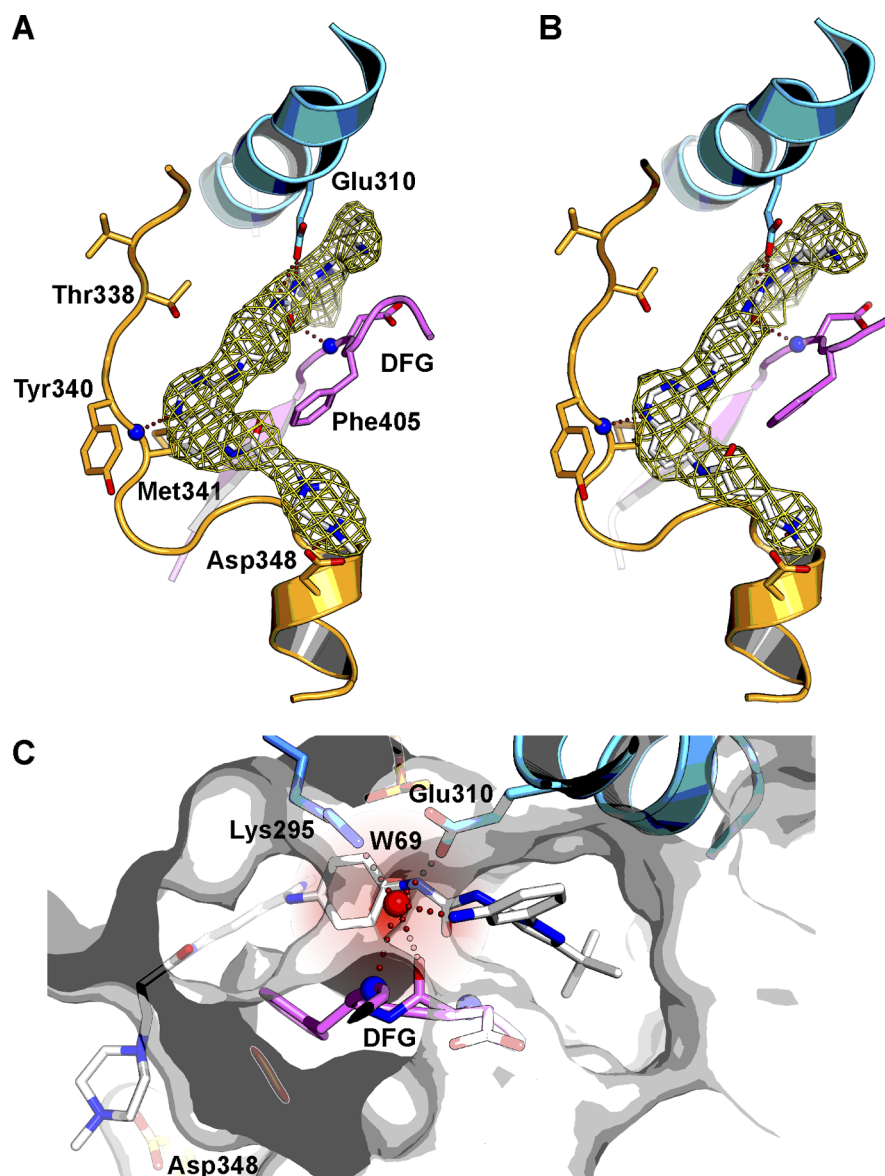


Figure 2. 1,4-Substituted hybrid compounds in complex with wild-type cSrc. Diagrams of the experimental electron densities of cSrc–3h at 2.7 Å (A) and cSrc–3g at 3.3 Å (B) resolution are shown ($2F_o - F_c$ map contoured at 1σ). Hydrogen-bond interactions of the inhibitors with helix C (turquoise), the DFG-motif (pink), and the hinge region (orange) are shown by red dotted lines. The kinase domain is in the inactive DFG-out conformation, and the pyrazolourea moiety resides in the allosteric site flanked by helix C and the DFG-motif. N1 of the quinazoline makes a direct hydrogen bond to the main chain amide of Met341, which is an interaction commonly formed between anilinoquinazolines and the hinge region of several other protein kinase domains. In both complexes, the central phenyl moiety that links the quinazoline scaffold with the pyrazolourea fragment interacts with the side chain of Phe405 (DFG motif) in a favorable edge-to-face orientation. (C) The aromatic amine points into a polar subpocket that is formed by three polar amino acid side chains (Lys295, Glu310, and Asp404) and forms polar interactions with a water molecule (red sphere). A detailed illustration of this interaction, including electron density data, is provided in Figure S2, Supporting Information.

in which we showed that the rigid 1,3-hybrid scaffold resulted in a steric repulsion between the gatekeeper residue and the inhibitor's central phenyl ring leading to a lower affinity against the mutant form of cSrc.³⁰ Derivatizing the quinazoline 6-amine resulted in increased potency versus related nonmodified structures (3f–i vs 3a–e). Except for 3c, equipped with a primary amine, the whole set of 1,4-fused hybrid compounds follows this general observation. Notably, there was no difference in efficacy observed between 3f and 3h (both ~1 nM), illustrating that an additional interaction to Asp348 is not obligatory for improved binding. Rather, the composition of quinazoline-6-amide and *meta*-amine is responsible for the observed effect.

Complex Crystal Structures of Type II Hybrids in cSrc.

To confirm the proposed general binding mode of our type II hybrids and to study the relevance of the newly introduced moieties we cocrystallized wild-type cSrc with 3g and 3h (Figure 2). As anticipated by the modeling results, these hybrid inhibitors were bound in a type II manner, accessing both allosteric and ATP-binding pockets, thereby locking the kinase in its inactive DFG-out conformation. Similar to the crystal structure of the parent compound (2a), the quinazoline N1 generates a direct hydrogen bond to the peptide backbone of Met341, located within the cSrc hinge region. The 1,4-fused phenyl ring of the inhibitor is sandwiched between the gatekeeper and Phe405 of the DFG motif, whereas the urea part is

embedded within the groove formed by helix C (stabilized by two hydrogen bonds to Glu310) and DFG motif (one hydrogen bond to Asp404). An additional interaction was created by the pyrazolo portion, which binds to the allosteric subpocket by forming a water-mediated hydrogen bond to Asp404 (Figure 2). The newly introduced 6-quinazoline substituents (4-(dimethylamino)-butanoic acid and 3-(4-methylpiperazin-1-yl)propanoic acid) contributed to the affinity by an additional hydrogen bond to Asp348. A novel protein ligand interaction was created by the inhibitor's primary amino moiety via a polar contact to a small polar subpocket, which is located outward of the allosteric site and is comprised by a water molecule (W69) and polar amino acid side chains (Lys295, Glu310, and the backbone of the DFG-motif, Figure 2C).

Hybrid Compounds Inhibit Drug-Resistant Mutants KIT V559D/T670I and Abl T315I. The results from activity-based studies on KIT and Abl were highly similar to those conducted with cSrc. Consistent with our previous studies, kinase selectivity profiling showed clear evidence for KIT as a possible target for our hybrid inhibitors.³⁰ Within the kinase domain of KIT, the same principal features are potentially addressable by our newly designed binders because comparison to cSrc and biochemical investigations revealed strong inhibition against its constitutively active (V559D) and concomitant gatekeeper mutated (T670I) form. We observed IC_{50} values in the low nanomolar range against KIT wild-type for **3b–d** and **3f–i** (2.6–7.6 nM) whereas the 1,3-fused inhibitors **4a** and **4b** were slightly less potent, eliciting values around 30 nM (Table 2). Consistent with the previous findings on cSrc, the more rigid compounds (**4a,b**) completely lost their inhibitory activity against the V559D/T670I mutant form. However, the activity of this double mutant was impeded by the bulk of the 1,4-fused compounds without significant loss of efficiency for most representatives (**3c** and **3g–i**, 2.7–9.2 nM) due to their adaptive phenyl ring, which most likely rotates by 90° and avoids a steric clash with the bulky gatekeeper (isoleucine). Strikingly, we observed a strong analog effect for **6a** and **6b** against KIT (1.0 and 4.5 nM), but the transfer of this effect to the gatekeeper mutant form was not achieved for **6b**, which exhibited a 1000-fold loss of potency, while **6a** revealed essentially no effect.

The 1,3-fused hybrid compounds **4a,b** showed a very high affinity for the Abl wild-type kinase (IC_{50} = 9–23 nM) whereas they completely failed to inhibit the T315I gatekeeper mutant form (Table 2). In contrast, the 1,4-fused hybrid compounds **3a–d** and **3f–h** exhibited a significant inhibition of wild-type Abl (IC_{50} = 42–157 nM) and predominantly retained their potency toward Abl T315I (IC_{50} = 81–176 nM). As seen in cSrc, fragments **5a,b** and scaffolds without the pyrazolo moiety **6a,b** showed no evidence of binding, suggesting that further interactions of this unique moiety were required for binding to Abl. Thus, our approach of using inhibitors with rotatable motifs to overcome gatekeeper mutations in kinases was successful for the *in vitro* inhibition of cSrc, KIT, and Abl (for biochemical selectivity profile of **3d** see Figure S3, Supporting Information).

Type II Inhibitors are Active on GIST Cell Lines Expressing KIT T670I. We investigated inhibitory effects of selected derivatives on human, untreated, metastatic GIST cells harboring a 57 bp deletion of exon 11, which leads to expression of constitutively activated KIT (GIST-T1).³⁵ Additionally, we examined the corresponding T670I gatekeeper mutated variant (GIST-T1 T670I) (Figure 3A,B,D). We treated each type of the cells for 72 h with **3b**, **3c**, **3d**, **3f**, **3h**, and **6b** (0–30 μ M);

imatinib and ponatinib served as control compounds. All tested compounds markedly reduced the number of viable GIST-T1 cells. In particular, **3b**, **3d**, and **6b**, without the quinazoline 6-position substitution, accounted for the most significant effects (GI_{50} = 11–17 nM). Substituted representatives (**3f,h**) as well as **3c**, carrying a primary amine at the 6-position, were somewhat less effective (GI_{50} = 105–402 nM). Treatment of imatinib-resistant GIST-T1 T670I cells generated a similar effect, showing the 1,4-fused quinazoline-pyrazolo urea hybrids to preserve their antiproliferative effects. The observed efficacies were comparable to those observed for GIST-T1 with **3b** and **3d**, which were the most potent derivatives (GI_{50} = 24–28 nM), followed by **3c** (110 nM).

Notably, a strong inhibitory effect was also observed for **6b** with respect to GIST-T1 T670I (GI_{50} = 121 nM). We observed an almost 8-fold discrepancy in the inhibition of the isolated protein KIT V559D/T670I (IC_{50} = 923 nM) versus the inhibition in the corresponding cell line by **6b**. Compound **6b** may represent a slow binder, possessing a slow on- and off-rate and therefore its true activity within a biochemical system may not be fully evident. The difference in efficacy may be related to the marginal incubation times with the isolated protein (0.5 h) compared with cellular systems (72 h). A cellular system represents an open equilibrium binding situation and a slow off-rate could potentially lead to temporal target selectivity.³⁶ Treatment of KIT-negative GIST-48B cells did not result in decreased proliferation, indicating no incidence of generic toxicity for the whole set of tested compounds with GI_{50} values ≥ 30 μ M except **3c**, **3f**, and **3h**, which did not elicit any anti-proliferative effect at concentrations up to 30 μ M (Figure 3C). Therefore, the tested molecules without exception revealed an improved off-target profile in GISTs compared with imatinib (GI_{50} = 20 μ M) and ponatinib (2.1 μ M), a phase III clinical candidate for treatment of CML.²⁴

In order to study the immediate impact on cellular KIT autophosphorylation and disruption of downstream signaling, we monitored phosphorylation states of KIT Y703 (autophosphorylation site) and the related downstream targets Akt (pS473) and MAPK (pT202/Y204) by Western blot analysis (Figure 3E,F). Treatment with **3d** and **3h** reduced cellular amounts of pKIT and simultaneously pAkt and pMAPK in GIST-T1 in a concentration-dependent manner. Applying 70 nM **3d** or 2000 nM **3h** led to 50% abrogation of the total amount of protein, confirming the direct effect of the hybrid compounds on KIT. The different substitution pattern of **3d** and **3h** led to different cellular performances (Figure 3A–D). Compound **3d** has no substituent on the quinazoline 6-position, whereas **3h** has an ethylenamide-linked methylpiperazine which apparently led to reduced efficacy by most likely increasing both polarity and molecular weight. This observation was accompanied by a similar reduction of pKIT and downstream signaling levels through pAkt and pMAPK caused by **3d** and **3h** at distinct concentrations (50% reduction of pKIT at 35 nM and 400 nM, respectively) in the corresponding GIST-T1 T670I cells expressing gatekeeper mutated KIT. However, these results confirmed our initial hypothesis on clinically relevant gatekeeper mutations to be overcome in a cellular system by equipping small molecules with elements which incorporate rotational flexibility.

Additional experiments were performed in order to investigate the inhibitory effect on Bcr-Abl and the respective T315I gatekeeper mutated species in Ba/F3 cells (Figure S4, Supporting Information). According to the biochemical investigations on isolated kinase domains, the 1,4-fused inhibitors

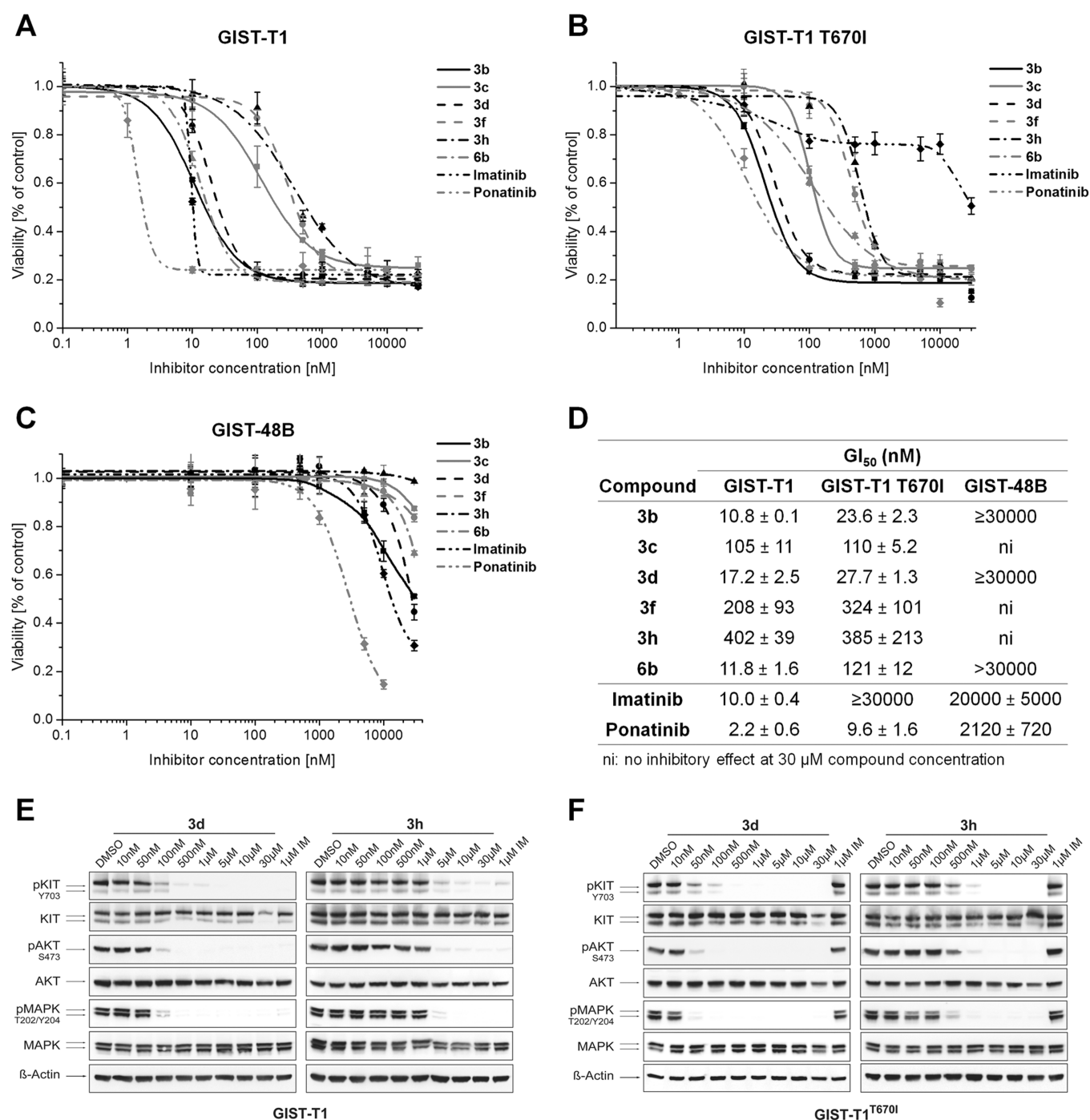


Figure 3. Dose–response curves of hybrid compounds on GIST cells expressing (A) constitutively active KIT (GIST-T1) as well as (B) the gatekeeper mutated KIT T670I (GIST-T1 T670I) and (C) the KIT negative cell line GIST-48B after 72 h incubation with the respective compounds; (D) GI₅₀ values on GIST-T1, GIST-T1 T670I, and GIST-48B; (E,F) Western blot analyses after 24 h of incubation with doses of 3d, 3h, and imatinib (IM) in GIST-T1 and GIST-T1 T670I.

were less potent. Nevertheless 3b and 3d were following the same trend reducing the viability of Ba/F3 Bcr-Abl cells (GI₅₀ = 4.1 μM and 4.3 μM) and furthermore retaining the antiproliferative effect on the gatekeeper resistant mutation in Ba/F3 Bcr-Abl T315I (GI₅₀ = 3.5 μM and 1.6 μM). Comparatively to the GIST studies, these results reflect the biochemical characterizations, which indicated that the inhibitory effect on KIT is more significant as compared with Abl.

Cytotoxicity and Inhibition of Metabolic Enzymes. In order to explore the hybrid compounds' general cytotoxicity

additional studies using liposarcoma (LPS141), leiomyosarcoma (LMS676), and malignant peripheral nerve sheath tumor cells (MPNST) were conducted (Figure S5, Supporting Information). There was no significant effect observed for the whole set of compounds. The most representative inhibitor, 3d, showed GI₅₀'s of around 15.1 μM (LPS141), 25.7 μM (LMS676), and 11.7 μM (MPNST), while its 6-position extended analogue 3h did not significantly decrease the number of viable cells up to inhibitor concentrations of 30 μM. Interestingly, the marketed drug ponatinib reduced the viability

of the respective cell lines to 50% at concentrations ranging from 0.1 to 0.8 μM . Next, we investigated the inhibitory impact of **3d** and **3h** on five CYPs (1A2, 2C9, 2C19, 2D6, and 3A4), as representative drug metabolizing enzymes and predictive markers for potential adverse effects (Table S2, Supporting Information). None of the tested cytochromes except 3A4 (IC_{50} = 14.8 μM and 1.95 μM for **3d** and **3h**) was remarkably inhibited.

DISCUSSION AND CONCLUSIONS

The emergence of drug resistance in kinases due to acquired secondary mutations, with the most considerable mutations affecting the gatekeeper residue, is a central challenge for developing novel inhibitors for the long-term treatment of cancer. Here, we present the development and optimization of 1,4-fused quinazoline–pyrazolourea hybrids by structure-based design to compose and synthesize a focused library of inhibitors. SAR studies showed an improved activity of hybrid compounds **3f–h** toward cSrc (IC_{50} \approx 1 nM) compared with initially published inhibitors. An enhanced effect toward cSrc resulted from the newly introduced *meta*-oriented amino moiety at the pyrazolo-phenyl ring whereas the formation of an extra hydrogen bond to the kinase apparently was not crucial for increased potency (Table 2, **3f** vs **3h**). Rather, the presence of a *meta*-amine and an obligatory amide at the quinazoline 6-position led to improved binding effects. These findings can be closely correlated to the enthalpy–entropy compensation caused by the entropically disfavored fixation of the ligand, for example in **3h**, which compensates the favorable enthalpic increase generated by the new hydrogen bond to Asp348 (Figure 2). The binding between the protein and the polar moiety of the inhibitor contributes to the desolvation energy by stripping away the hydration shell. In the case of compounds **3g–i**, the surrounding tertiary amines represent an energetic barrier that must be overcome.³⁷ In addition, we achieved the transfer of the inhibitory activity onto stem cell factor receptor KIT (wild-type and V559D/T670I mutant, IC_{50} = 3–8 nM and 3–38 nM, respectively, for **3b–d**, **3f–i**), as well as Abl kinase (wild-type and T315I mutant, IC_{50} = 40–157 nM and 81–561 nM, respectively, for **3a–d,h**). The preserved inhibitory effects with respect to gatekeeper mutated kinases bearing bulky substituents on that position was likewise due to the spatial arrangement of the rotatable 1,4-fused phenyl ring connecting the inhibitor's type I and type III parts. A 90° axial rotation of this element, as shown for addressing the T338M gatekeeper mutated form of cSrc,³⁰ likewise accounted for the potent inhibition of the corresponding mutated kinases KIT T670I and Abl T315I.

In cellular characterizations, we further extended the hybrids' impact from significant *in vitro* inhibition of wild-type KIT as well as the gatekeeper and its simultaneously activating mutant form (V559D/T670I) to addressing the relevant stem cell factor receptor kinase species in human, untreated, metastatic GIST-T1 cells and, particularly, the KIT T670I positive cell line GIST-T1 T670I. We observed a significant impact in reduction of viable GIST-T1 (GI_{50} = 11–17 nM for **3b/d**, **6b**) cells and moreover the inhibitory effect was maintained in GIST-T1 T670I (GI_{50} = 24–121 nM for **3b/d**, **6b**) cells. The latter observation underlines our successful approach to generate hybrid compounds containing motifs with rotational flexibility that can override the mutations of gatekeeper residues in a cellular system. Notably, the inhibitory effect for compounds lacking further substitutions at the quinazoline

6-position (**3b/d**, **6b**) was superior to the effect of compounds bearing an extension (**3f/h**), suggesting that additional interactions with Asn680 (located at the lip of the hinge region) are not necessary at the cellular level, which agrees with the concept of enthalpy–entropy compensation. Furthermore, the introduction of polar moieties may affect the capability of the compounds to pass through the cell membrane, which may result in the generation of less significant cellular concentrations and thereby reduced potency of the quinazoline 6-position substituted compounds.

The presented hybrid derivatives exhibit enormous potential in the therapeutic treatment of solid GISTs through addressing gain of function mutants of KIT, and due to their central and rotatable element they are similarly able to target the gatekeeper mutated T670I species. A recently released study by O'Hare et al. demonstrated that a linear triple bond as a connecting structural element between type I and type III like binders is likewise useful to overcome gatekeeper mutations in Abl due to its decreased spatial arrangement.³⁸ Derivatives harboring this structural motif were shown to conserve their inhibitory effect even against the T315I gatekeeper mutant form in xenograft models, and one representative (ponatinib) is now in phase III clinical trials as a pan-Bcr-Abl inhibitor for CML treatment.^{24,38} Recently the FDA granted accelerated approval for ponatinib in the treatment of CML with resistance or intolerance to prior tyrosine kinase inhibitor therapy. However, severe side effects with hepatotoxicity leading to liver failure and death in some cases and 8–11% of treated patients revealing arterial thrombosis, were observed in clinical trials, indicating a rather complex pharmacology.³⁹

In conclusion, our previously described quinazoline–pyrazolourea hybrids were optimized by using methods of medicinal chemistry. Using initial modeling studies and evaluating the improved effect by biochemical characterizations, we successfully obtained substantial transferability of the preliminarily determined binding mode to the clinically relevant kinases KIT and Abl. Furthermore, their constitutively active variants and gatekeeper mutants (T670I of KIT and T315I of Abl) were significantly inhibited as shown in biochemical characterizations using isolated kinase domains. Finally, compounds **3b**, **3c**, **3d**, **3f**, **3h**, and **6b** exhibit strong antiproliferative effects in cells derived from solid tumors harboring constitutively active KIT (GIST-T1) as well as gatekeeper mutated KIT T670I (GIST-T1 T670I) variants and thus represent valuable starting points for future medicinal chemistry endeavors.

EXPERIMENTAL SECTION

Chemistry. Unless otherwise noted, all reagents and solvents were purchased from Acros, Fluka, Sigma-Aldrich, or Merck and used without further purification. Dry solvents were purchased as anhydrous reagents from commercial suppliers. ^1H and ^{13}C NMR spectra were recorded on a Bruker Avance DRX 400 spectrometer at 400 and 101 MHz, respectively. ^1H chemical shifts are reported in δ (ppm) as s (singlet), d (doublet), dd (doublet of doublet), t (triplet), q (quartet), m (multiplet), and bs (broad singlet) and are referenced to the residual solvent signal: CDCl_3 (7.26) or $\text{DMSO}-d_6$ (2.50). ^{13}C spectra are referenced to the residual solvent signal: CDCl_3 (77.16) or $\text{DMSO}-d_6$ (39.52). High-resolution electrospray ionization mass spectra (ESI-FTMS) were recorded on a Thermo LTQ Orbitrap (high-resolution mass spectrometer from Thermo Electron) coupled to an "Accela" HPLC system supplied with a "Hypersil GOLD" column (Thermo Electron). Analytical TLC was carried out on Merck 60 F245 aluminum-backed silica gel plates. Compounds were purified by column chromatography using Baker silica gel (40–70 μm particle size). Preparative HPLC was conducted on a Varian HPLC system

(Pro Star 215) with a VP 250/21 nucleosil C18 PPN column from Macherey-Nagel and monitored by UV at $\lambda = 254$ nm. All final compounds were purified to $\geq 95\%$ purity confirmed by LCMS analysis on LCQ Advantage MAX (1200 series, Agilent) with Eclipse XDB-C18-column (5 μ M, 150 \times 1.6 mm, Phenomenex).

3-tert-Butyl-1-(3-nitrophenyl)-1H-pyrazol-5-amine Hydrochloride (7). A solution of *m*-nitrophenylhydrazine hydrochloride (2.00 g, 10.55 mmol) and pivaloylacetone nitrile (1.53 g, 11.88 mmol) in dry EtOH (22 mL) was treated with concentrated HCl (3 mL) and refluxed for 12 h at 90 °C. The precipitate was filtered off and dried under reduced pressure before the crude was recrystallized from plain hexane yielding 2.94 g (9.91 mmol, 94%) of white crystals: ^1H NMR (400 MHz, CDCl_3) δ 8.45 (t, $J = 2.1$ Hz, 1H), 8.09 (m, 2H), 7.73 (t, $J = 8.2$ Hz, 1H), 5.48 (bs, 2H), 5.47 (s, 1H), 1.23 (s, 9H); ^{13}C NMR (101 MHz, CDCl_3) δ 162.12, 148.09, 147.96, 140.59, 130.48, 127.70, 119.59, 115.99, 88.22, 31.93, 30.03. HRMS (ESI-MS) calcd: 261.13460 for $\text{C}_{13}\text{H}_{17}\text{N}_4\text{O}_2$ [$\text{M} + \text{H}^+$]. Found: 261.13456.

2,2,2-Trichloroethyl 1-(3-nitrophenyl)-1H-pyrazol-5-ylcarbamate (8). NaOH (1.13 g, 28.3 mmol) was added to a suspension of 7 (2.94 g, 11.3 mmol) in EtOAc (20 mL) and H_2O (6 mL) at 0 °C. The resulting reaction mixture was stirred for 30 min before 2,2,2-trichloroethyl chloroformate (2.28 mL, 17.0 mmol) was added dropwise. After an additional 30 min, the mixture was warmed to room temperature and stirred for 3 h. The organic layer was separated from the aqueous layer, which then was extracted with EtOAc (3 \times 25 mL). The combined organic layers were once washed with brine, dried over Na_2SO_4 , and concentrated under reduced pressure. Purification of the crude by silica gel column chromatography (20% EtOAc/petrol ether) lead to 4.79 g (11.0 mmol, 97%) of the desired product as a brown resin: ^1H NMR (400 MHz, CDCl_3) δ 8.37 (s, 1H), 8.17 (dd, $J = 8.1, 1.2$ Hz, 1H), 7.88 (dd, $J = 8.1$ Hz, 1H), 7.60–7.65 (m, 1H), 6.35 (s, 1H), 4.76 (s, 2H), 3.08 (s, 1H), 1.33 (s, 9H); ^{13}C NMR (101 MHz, CDCl_3) δ 163.56, 148.76, 139.44, 134.81, 130.48, 130.00, 122.31, 119.29, 99.55, 94.84, 76.32, 75.14, 32.72, 30.28. HRMS (ESI-MS) calcd: 435.03881 for $\text{C}_{16}\text{H}_{18}\text{Cl}_3\text{N}_4\text{O}_4$ [$\text{M} + \text{H}^+$]. Found: 435.03874.

1-(3-tert-Butyl-1-(3-nitrophenyl)-1H-pyrazol-5-yl)-3-methylurea (4a). A suspension of 8 (100 mg, 0.23 mmol), methylamine hydrochloride (155 mg, 230 mmol), and DIPEA (393 μ L) in DMSO (2 mL) was stirred for 5 h at room temperature. Saturated sodium-bicarbonate solution was added, and the resulting mixture was extracted with EtOAc (5 \times 15 mL). The combined organic layers were dried over Na_2SO_4 , and the volatiles were removed in vacuo. The crude was purified on silica gel using 0.5% MeOH/DCM which lead to 59 mg (0.19 mmol, 83%) of the desired product as a light yellow solid: ^1H NMR (400 MHz, $\text{DMSO}-d_6$) δ 8.39 (s, 1H), 8.32 (t, $J = 2.1$ Hz, 1H), 8.19 (ddd, $J = 8.2, 2.2, 0.8$ Hz, 1H), 8.00 (ddd, $J = 8.0, 1.9, 0.8$ Hz, 1H), 7.78 (t, $J = 8.2$ Hz, 1H), 6.40–6.33 (m, 1H), 6.29 (s, 1H), 2.58 (d, $J = 4.6$ Hz, 3H), 1.28 (s, 9H); ^{13}C NMR (101 MHz, $\text{DMSO}-d_6$) δ 161.75, 155.33, 148.03, 139.84, 138.45, 130.65, 129.21, 121.06, 117.46, 98.23, 32.13, 30.03, 26.41. HRMS (ESI-MS) calcd: 318.15607 for $\text{C}_{15}\text{H}_{20}\text{N}_5\text{O}_3$ [$\text{M} + \text{H}^+$]. Found: 318.15611.

1-(1-(3-Aminophenyl)-3-tert-butyl-1H-pyrazol-5-yl)-3-methylurea (4b). A solution of 4a (104 mg, 0.33 mmol) and ammonium formate (124 mg, 1.97 mmol) in EtOH (7 mL) was treated with 5% Pd on charcoal (70 mg, 33 μ mol). The resulting reaction mixture was refluxed for 1 h at 90 °C before the catalyst was filtered off and the volatiles were removed under reduced pressure. The crude was purified on silica gel (2% MeOH/DCM) yielding 67 mg (0.23 mmol, 70%) of a white solid: ^1H NMR (400 MHz, $\text{DMSO}-d_6$) δ 8.09 (s, 1H), 7.10 (t, $J = 7.9$ Hz, 1H), 6.66 (t, $J = 1.9$ Hz, 1H), 6.60–6.52 (m, 2H), 6.43 (q, $J = 4.1$ Hz, 1H), 6.22 (s, 1H), 5.36 (s, 2H), 2.61 (d, $J = 4.6$ Hz, 3H), 1.25 (s, 9H); ^{13}C NMR (101 MHz, $\text{DMSO}-d_6$) δ 159.99, 154.75, 149.62, 139.31, 137.83, 129.32, 112.63, 111.21, 109.77, 94.01, 31.94, 30.27, 26.21. HRMS (ESI-MS) calcd: 288.18189 for $\text{C}_{15}\text{H}_{22}\text{N}_5\text{O}$ [$\text{M} + \text{H}^+$]. Found: 288.18188.

General Procedure for the Preparation of *N*-Boc-Aminophenyl-3-(3-tert-butyl-1-(3-nitrophenyl)-1H-pyrazol-5-yl)ureas (9, 10). DIPEA was added to a solution of *N*-Boc-phenylenediamine in abs. DMSO and stirred under argon atmosphere at room temperature for 5 min. After addition of 8 in one portion, the resulting reaction mixture was stirred for 24 h at 60 °C. After cooling to room temperature, the mixture was poured

into saturated bicarbonate solution followed by extraction with EtOAc (3 \times 20 mL). The combined organic layers were dried over Na_2SO_4 , and the volatiles were removed under reduced pressure. The crude was purified by silica gel column chromatography.

tert-Butyl 4-(3-(3-tert-Butyl-1-(3-nitrophenyl)-1H-pyrazol-5-yl)-ureido)phenylcarbamate (9). Compound 9 was prepared as described in the general procedure using *tert*-butyl 4-aminophenylcarbamate (1.43 g, 6.88 mmol), DMSO (25 mL), DIPEA (2.36 mL, 13.8 mmol), and 8 (3 g, 6.88 mmol). The crude material was purified on silica gel (20–50% EtOAc/petrol ether) to yield 2.07 g (4.19 mmol, 61%) of a light yellow solid: ^1H NMR (400 MHz, $\text{DMSO}-d_6$) δ 8.23 (s, 1H), 7.98 (d, $J = 8.0$ Hz, 1H), 7.80 (s, 2H), 7.72 (d, $J = 7.7$ Hz, 1H), 7.44–7.40 (m, 1H), 7.10 (d, $J = 8.4$ Hz, 2H), 6.99 (d, $J = 8.6$ Hz, 2H), 6.58 (s, 1H), 6.38 (s, 1H), 1.45 (s, 9H), 1.28 (s, 9H); ^{13}C NMR (101 MHz, $\text{DMSO}-d_6$) δ 163.56, 151.93, 148.79, 139.40, 134.82, 130.51, 130.02, 122.36, 119.33, 99.55, 94.83, 76.35, 75.17, 60.73, 32.74, 30.29, 26.26, 21.24, 14.32. HRMS (ESI-MS) calcd: 495.23504 for $\text{C}_{25}\text{H}_{31}\text{N}_6\text{O}_3$ [$\text{M} + \text{H}^+$]. Found: 495.23445.

tert-Butyl 3-(3-(3-tert-Butyl-1-(3-nitrophenyl)-1H-pyrazol-5-yl)-ureido)phenylcarbamate (10). Compound 10 was prepared as described in the general procedure using *tert*-butyl 3-aminophenylcarbamate (300 mg, 0.69 mmol), DMSO (3 mL), DIPEA (236 μ L, 1.38 mmol), and 8 (144 mg, 0.69 mmol). The crude material was purified on silica gel (0–0.5% MeOH/DCM) to yield 276 mg (0.56 mmol, 81%) of a light yellow solid: ^1H NMR (400 MHz, $\text{DMSO}-d_6$) δ 9.32 (s, 1H), 9.05 (s, 1H), 8.46 (s, 1H), 8.36 (t, $J = 2.1$ Hz, 1H), 8.22 (dd, $J = 8.2, 1.5$ Hz, 1H), 8.08–8.02 (m, 1H), 7.81 (t, $J = 8.2$ Hz, 1H), 7.57 (s, 1H), 7.11 (dd, $J = 7.7, 4.5$ Hz, 2H), 7.00–6.95 (m, 1H), 6.42 (s, 1H), 1.46 (s, 9H), 1.30 (s, 9H); ^{13}C NMR (101 MHz, $\text{DMSO}-d_6$) δ 161.94, 152.70, 151.74, 148.14, 139.97, 139.61, 139.59, 137.80, 130.83, 129.57, 128.92, 121.42, 117.97, 112.28, 112.03, 108.07, 97.59, 79.01, 32.19, 30.07, 28.14. HRMS (ESI-MS) calcd: 495.23504 for $\text{C}_{25}\text{H}_{31}\text{N}_6\text{O}_3$ [$\text{M} + \text{H}^+$]. Found: 495.23443.

tert-Butyl 4-(3-(((9H-Fluoren-9-yl)methoxy)carbonylamino)-phenyl)-3-tert-butyl-1H-pyrazol-5-yl)ureido)phenylcarbamate (11, 2 steps). In a dry and argon-flushed flask, a solution of 9 (960 mg, 1.35 mmol) in EtOH (6 mL) was treated with ammoniumformate (510 mg, 8.1 mmol) and 5% Pd on charcoal (297 mg, 0.14 mmol) for 1 h at 70 °C. After filtration of the reaction mixture over Celite, the solvents were removed in vacuo. Recrystallization of the crude product from hexane resulted in 608 mg (1.31 mmol, 97%) of a pink solid, which was used without further purification: ^1H NMR (400 MHz, $\text{DMSO}-d_6$) δ 9.29 (s, 1H), 9.19 (s, 1H), 8.62 (s, 1H), 7.30 (q, $J = 9.1$ Hz, 4H), 7.13–7.09 (m, 1H), 6.69–6.68 (m, 1H), 6.62–6.53 (m, 2H), 6.30 (s, 1H), 5.37 (s, 2H), 1.46 (s, 9H), 1.26 (s, 9H); ^{13}C NMR (101 MHz, $\text{DMSO}-d_6$) δ 160.94, 158.51, 153.68, 150.52, 148.16, 145.64, 140.02, 138.14, 134.99, 133.42, 130.27, 119.30, 113.64, 112.17, 110.73, 36.26, 32.83, 31.12, 29.02. HRMS (ESI-MS) calcd: 465.26087 for $\text{C}_{25}\text{H}_{33}\text{N}_6\text{O}_3$ [$\text{M} + \text{H}^+$]. Found: 465.26040.

NaHCO_3 (336 mg, 4.0 mmol) and Fmoc-Cl (297 mg, 0.14 mmol) were added to a suspension of the previously synthesized amine in water/dioxane (12 mL/17 mL), and the resulting reaction mixture was stirred overnight at room temperature. After addition of another 10 mL of water, the mixture was extracted with EtOAc (5 \times 30 mL). The combined organic layers were dried over Na_2SO_4 , and the volatiles were removed under reduced pressure. The crude product was purified on silica gel (2% MeOH/DCM) resulting in 833 mg (1.21 mmol, 76%) of a pink resin: ^1H NMR (400 MHz, $\text{DMSO}-d_6$) δ 9.96 (s, 1H), 9.21 (s, 1H), 8.86 (s, 1H), 8.34 (s, 1H), 7.91 (d, $J = 7.5$ Hz, 2H), 7.75 (d, $J = 7.5$ Hz, 2H), 7.63 (s, 1H), 7.54 (bs, 1H), 7.44–7.40 (t, $J = 7.3$ Hz, 3H), 7.38–7.31 (m, 4H), 7.28 (d, $J = 9.0$ Hz, 2H), 7.13 (d, $J = 7.5$ Hz, 1H), 6.36 (s, 1H), 4.51 (d, $J = 6.5$ Hz, 2H), 4.31 (t, $J = 6.5$ Hz, 1H), 1.46 (s, 9H), 1.27 (s, 9H); ^{13}C NMR (101 MHz, $\text{DMSO}-d_6$) δ 160.78, 153.38, 152.84, 151.33, 143.72, 140.82, 140.01, 138.80, 137.46, 134.80, 134.12, 133.80, 129.60, 127.71, 127.15, 125.13, 120.22, 118.64, 118.22, 114.38, 94.37, 91.87, 78.79, 65.68, 46.60, 32.04, 30.21, 28.17. HRMS (ESI-MS) calcd: 687.32894 for $\text{C}_{40}\text{H}_{43}\text{N}_6\text{O}_5$ [$\text{M} + \text{H}^+$]. Found: 687.32825.

(9H-Fluoren-9-yl)methyl 3-(3-tert-Butyl-5-(3-(4-(6-nitroquinazolin-4-ylamino)phenyl)ureido)-1H-pyrazol-1-yl)phenylcarbamate (12, 2 steps). A solution of 11 (814 mg, 1.19 mmol) in dioxane (2 mL) was treated

with HCl (8 mL, 4 M in dioxane) for 2 h at rt. After the reaction was completed, the volatiles were removed under reduced pressure and subsequently EtOAc (10 mL) and saturated sodium bicarbonate solution (10 mL) were added. The aqueous layer was extracted with EtOAc (3 × 20 mL), and the combined organic layers were dried over Na₂SO₄. The solvent was removed in vacuo leading to 686 mg (1.17 mmol, 98%) of a light yellow solid, which was used without further purification: ¹H NMR (400 MHz, DMSO-*d*₆) δ 9.96 (s, 1H), 8.50 (s, 1H), 8.22 (s, 1H), 7.91 (d, *J* = 7.5 Hz, 2H), 7.76 (d, *J* = 7.4 Hz, 2H), 7.63 (s, 1H), 7.55 (s, 1H), 7.47–7.31 (m, 6H), 7.12 (d, *J* = 7.6 Hz, 1H), 7.03 (d, *J* = 8.7 Hz, 2H), 6.49 (d, *J* = 8.7 Hz, 2H), 6.33 (s, 1H), 4.84 (s, 2H), 4.51 (d, *J* = 6.5 Hz, 2H), 1.26 (s, 9H); ¹³C NMR (101 MHz, DMSO-*d*₆) δ 160.73, 153.38, 151.55, 144.12, 143.73, 140.82, 139.99, 138.87, 137.81, 129.57, 128.27, 127.72, 127.15, 125.14, 120.46, 120.22, 118.20, 114.36, 114.14, 94.09, 91.54, 65.69, 46.60, 32.03, 30.22. HRMS (ESI-MS) calcd: 587.27652 for C₃₅H₃₅N₆O₃ [M + H⁺]. Found: 587.27588.

A solution of the previously synthesized amino hydrochloride (739 mg, 1.26 mmol) in DCM (33 mL) under argon atmosphere was treated with DIPEA (1 mL, 5.84 mmol) for 10 min at rt. Thereafter freshly prepared 4-chloro-6-nitroquinazolinol (317 mg, 1.51 mmol) was added, and the resulting reaction mixture was stirred for 22 h at rt. After addition of saturated sodium bicarbonate solution and separation of the phases, the aqueous layer was extracted with DCM (3 × 50 mL). The combined organic layers were dried over Na₂SO₄, and the volatiles were removed under reduced pressure. The crude material was purified on silica gel (1–4% MeOH/DCM) yielding 743 mg (0.97 mmol, 77%) of the desired product as a yellow-orange solid: ¹H NMR (400 MHz, DMSO-*d*₆) δ 10.41 (s, 1H), 9.98 (s, 1H), 9.64 (s, 1H), 9.07 (s, 1H), 8.66 (s, 1H), 8.54 (dd, *J* = 9.2, 2.3 Hz, 1H), 8.44 (s, 1H), 7.95–7.84 (m, 3H), 7.74 (dd, *J* = 14.2, 8.2 Hz, 4H), 7.67 (s, 1H), 7.55 (s, 1H), 7.47 (d, *J* = 8.9 Hz, 2H), 7.43–7.40 (m, 3H), 7.34 (t, *J* = 7.1 Hz, 2H), 7.16 (d, *J* = 7.7 Hz, 1H), 6.40 (s, 1H), 4.51 (d, *J* = 6.5 Hz, 2H), 4.31 (t, *J* = 6.5 Hz, 1H), 1.28 (s, 9H); ¹³C NMR (101 MHz, DMSO-*d*₆) δ 160.80, 158.68, 157.85, 153.39, 153.13, 151.39, 144.42, 143.72, 140.81, 140.03, 138.82, 137.35, 136.13, 132.63, 129.62, 129.41, 127.71, 127.14, 126.56, 125.14, 123.65, 120.84, 120.21, 118.26, 118.23, 118.19, 114.39, 94.67, 65.70, 60.85, 46.60, 32.07, 30.22. HRMS (ESI-MS) calcd: 760.29904 for C₄₃H₃₈N₉O₅ [M + H⁺]. Found: 760.30027.

(9H-Fluoren-9-yl)methyl 3-(5-(3-(4-(6-Aminoquinazolin-4-ylamino)phenyl)ureido)-3-tert-butyl-1H-pyrazol-1-yl)phenylcarbamate (**3e**). Iron turnings (269 mg, 4.56 mmol) were activated, by treating them two times with 1 N HCl for 20 min at room temperature, and added to a suspension of **12** (434 mg, 0.57 mmol) in EtOH (40 mL) and AcOH (0.13 mL, 2.28 mmol). The resulting reaction mixture was refluxed for 2.5 h. After removal of the iron turnings, the remaining solution was basified with aqueous NH₃. The solvents were removed under reduced pressure, and the residue was dissolved with EtOAc and saturated sodium bicarbonate solution. Subsequently, the aqueous layer was extracted with EtOAc (10 × 40 mL), and the combined organic layers were dried over Na₂SO₄. The crude was purified on silica gel (4–6% MeOH/DCM) leading to 316 mg (0.43 mmol, 75%) of an off yellow solid: ¹H NMR (400 MHz, DMSO-*d*₆) δ 9.98 (s, 1H), 9.29 (s, 1H), 8.99 (s, 1H), 8.42 (s, 1H), 8.28 (s, 1H), 7.90 (d, *J* = 7.5 Hz, 2H), 7.80–7.70 (m, 4H), 7.66 (s, 1H), 7.55 (s, 1H), 7.51 (d, *J* = 8.8 Hz, 1H), 7.47–7.38 (m, 5H), 7.37–7.33 (m, 3H), 7.22 (dd, *J* = 8.9, 2.0 Hz, 1H), 7.16 (d, *J* = 7.8 Hz, 1H), 6.39 (s, 1H), 5.56 (s, 2H), 4.51 (d, *J* = 6.5 Hz, 2H), 4.32 (t, *J* = 6.5 Hz, 1H), 1.28 (s, 9H); ¹³C NMR (101 MHz, DMSO-*d*₆) δ 160.80, 156.04, 153.40, 151.40, 149.97, 147.16, 143.73, 142.36, 140.82, 140.03, 138.83, 137.47, 134.68, 134.37, 133.68, 129.62, 128.55, 127.72, 127.15, 125.14, 123.43, 122.57, 120.22, 118.26, 116.90, 116.59, 114.41, 101.14, 94.49, 65.69, 46.61, 32.06, 30.23. HRMS (ESI-MS) calcd: 730.32486 for C₄₃H₄₀N₉O₅ [M + H⁺]. Found: 730.32501.

N-(4-(4-(3-(1-(3-Aminophenyl)-3-tert-butyl-1H-pyrazol-5-yl)-ureido)phenylamino)quinazolin-6-yl)propanamide (**3f**). A solution of **3e** (50 mg, 68.5 μmol) in abs. THF (4 mL) under argon atmosphere was cooled to 0 °C before DIPEA (23.4 μL, 137 μmol) was added. Subsequently a diluted solution of propionylchloride (7.45 μL, 82.2 μmol) in THF (7.45 mL) was added dropwise over 45 min. After addition was completed, the resulting reaction mixture was stirred

for 10 min at 0 °C and for 1 h at room temperature. The volatiles were removed in vacuo, and the remaining solid was dissolved in EtOAc and saturated sodium bicarbonate solution. The aqueous layer was extracted with EtOAc (3 × 15 mL), and the combined organic layers were dried over Na₂SO₄. After that, the volatiles were evaporated under reduced pressure leading to 73 mg of a yellow-green crude product, which was used without further purification.

The remaining solid (69 mg) was treated with morpholine (1 mL, 30% in DMF) for 15 min at room temperature. Afterward, the solvents were removed under reduced pressure, and the crude was purified on silica gel using 10% MeOH/DCM. The resulting yellow solid was dissolved in THF and filtered through a membrane filter. After removal of the solvent under reduced pressure, 32 mg (56.8 μmol, 83%) of the desired yellow solid was isolated: ¹H NMR (400 MHz, DMSO-*d*₆) δ 10.20 (s, 1H), 9.73 (s, 1H), 9.14 (s, 1H), 8.69 (s, 1H), 8.45 (s, 1H), 8.37 (s, 1H), 7.81 (dd, *J* = 9.0, 1.9 Hz, 1H), 7.72 (d, *J* = 8.9 Hz, 1H), 7.68 (d, *J* = 8.9 Hz, 2H), 7.43 (d, *J* = 8.9 Hz, 2H), 7.18–7.14 (m, 1H), 6.70 (d, *J* = 1.9 Hz, 1H), 6.61 (dd, *J* = 8.0, 1.7 Hz, 2H), 6.37 (s, 1H), 5.42 (s, 2H), 2.41 (q, *J* = 7.5 Hz, 2H), 1.27 (s, 9H), 1.14 (t, *J* = 7.5 Hz, 3H); ¹³C NMR (101 MHz, DMSO-*d*₆) δ 172.12, 160.23, 157.91, 157.50, 153.29, 151.27, 149.81, 146.35, 139.08, 137.22, 136.76, 135.32, 133.73, 129.58, 128.21, 123.30, 118.12, 115.40, 112.97, 111.92, 111.50, 110.02, 93.54, 32.02, 30.30, 29.39, 9.66. HRMS (ESI-MS) calcd: 564.28300 for C₃₁H₃₄N₉O₂ [M + H⁺]. Found: 564.28278.

General Procedure for the Preparation of 1,4-Fused Hybrid Derivatives (3g–i). (COCl)₂ and catalytic amounts of DMF were added to a suspension of the appropriate acid of choice in THF or DCM under an argon atmosphere. The resulting mixture was stirred for 2 h at 30–35 °C before **13**, dissolved in 1–2 mL of NMP, was added in one portion. After another hour of stirring at room temperature, the reaction was completed. Subsequently saturated sodium bicarbonate solution was added and the aqueous layer extracted with EtOAc (3 × 20 mL). The combined organic layers were dried over Na₂SO₄ and the volatiles removed under reduced pressure. Treatment of the crude with a solution of 20–25% morpholine in THF or THF/DMF (4:1) for 30–60 min led to the removal of the Fmoc protecting group. After evaporation of the solvents in vacuo, the crude was purified by HPLC.

N-(4-(4-(3-(1-(3-Aminophenyl)-3-tert-butyl-1H-pyrazol-5-yl)-ureido)phenylamino)quinazolin-6-yl)-4-(dimethylamino)butanamide (**3g**). Compound **3g** was prepared as described in the general procedure using THF (3 mL), 4-(dimethylamino)butanoic acid (100 mg, 597 μmol), (COCl)₂ (52.3 μL, 597 μmol), DMF (two drops), and **3e** (50 mg, 68.5 μmol) in 1 mL of NMP. Deprotection was performed by treating the crude material with 20% morpholine in THF (2.4 mL) for 40 min. The volatiles were removed under reduced pressure, and the crude product was purified by preparative HPLC (H₂O/MeCN + 0.1% TFA). The combined, product containing fractions were concentrated under reduced pressure and subsequently basified with saturated sodium bicarbonate solution. After extraction of the aqueous layer with EtOAc (3 × 15 mL), drying of the combined organic layers over Na₂SO₄, and evaporation of the residual solvent in vacuo, 27 mg (43.5 μmol, 64%) of the desired product was isolated as a light green solid: ¹H NMR (600 MHz, DMSO-*d*₆) δ 10.22 (s, 1H), 9.70 (s, 1H), 9.12 (s, 1H), 8.67 (d, *J* = 1.6 Hz, 1H), 8.45 (s, 1H), 8.36 (s, 1H), 7.82 (d, *J* = 2.1 Hz, 1H), 7.72 (d, *J* = 8.9 Hz, 1H), 7.69 (d, *J* = 8.9 Hz, 2H), 7.45–7.40 (m, 2H), 7.16 (t, *J* = 7.9 Hz, 1H), 6.70 (t, *J* = 2.1 Hz, 1H), 6.62–6.61 (t, *J* = 2.4 Hz, 1H), 6.61–6.60 (t, *J* = 2.2 Hz, 1H), 6.36 (s, 1H), 5.39 (s, 2H), 2.42 (t, *J* = 7.4 Hz, 2H), 2.37 (t, *J* = 7.4 Hz, 2H), 2.22 (s, 6H), 1.79 (p, *J* = 7.4 Hz, 2H), 1.27 (s, 9H); ¹³C NMR (101 MHz, DMSO-*d*₆) δ 171.14, 160.17, 157.46, 153.24, 151.25, 149.73, 146.34, 139.07, 137.17, 136.69, 135.29, 133.70, 129.49, 128.15, 124.87, 123.25, 118.10, 115.35, 112.92, 111.88, 111.45, 109.99, 93.55, 58.23, 44.79, 31.95, 30.40, 30.24, 22.59. HRMS (ESI-MS) calcd: 621.34085 for C₃₄H₄₁N₁₀O₂ [M + H⁺]. Found: 621.34078.

N-(4-(4-(3-(1-(3-Aminophenyl)-3-tert-butyl-1H-pyrazol-5-yl)-ureido)phenylamino)quinazolin-6-yl)-3-(4-methylpiperazin-1-yl)propanamide-TFA (**3h**). Compound **3h** was prepared as described in the general procedure using DCM (3 mL), 3-(4-methylpiperazin-1-yl)propanoic acid (35 mg, 200 μmol), (COCl)₂ (17.5 μL, 200 μmol), DMF (three drops), and **3e** (50 mg, 68.5 μmol) in NMP (1.5 mL).

Treatment of the crude with a solution of 20% morpholine in THF/DMF (5 mL, 4:1) for 1 h led to the removal of the Fmoc protecting group. After evaporation of the volatiles under reduced pressure, the crude product was purified by preparative HPLC (H₂O/MeCN + 0.1% TFA) yielding 23 mg (29.6 μ mol, 43%) of the desired product as a yellow solid: ¹H NMR (400 MHz, DMSO-*d*₆) δ 11.53 (s, 1H), 10.85 (s, 1H), 9.46 (s, 1H), 8.98 (s, 1H), 8.85 (s, 1H), 8.72 (s, 1H), 8.07 (d, *J* = 9.1 Hz, 1H), 7.89 (d, *J* = 9.0 Hz, 1H), 7.55 (q, *J* = 9.2 Hz, 4H), 7.35 (t, *J* = 8.0 Hz, 2H), 7.09 (s, 1H), 7.05 (d, *J* = 8.1 Hz, 1H), 6.92 (d, *J* = 7.9 Hz, 2H), 6.37 (s, 1H), 3.34 (s, 2H), 3.34 (bs, 8H), 2.94–2.87 (m, 2H), 2.86 (s, 3H), 1.28 (s, 9H); ¹³C NMR (101 MHz, DMSO-*d*₆) δ 168.87, 160.75, 159.31, 159.16, 158.80, 158.45, 158.10, 151.72, 149.70, 139.38, 138.75, 138.19, 137.17, 134.60, 130.68, 129.97, 125.51, 120.58, 118.12, 117.45, 116.54, 114.54, 113.97, 112.74, 95.77, 51.49, 50.19, 48.58, 41.99, 32.09, 31.44, 30.22. HRMS (ESI-MS) calcd: 662.36740 for C₃₆H₄₄N₁₁O₂ [M + H⁺]. Found: 662.36721.

N-(4-(4-(3-(1-(3-Aminophenyl)-3-*tert*-butyl-1H-pyrazol-5-yl)ureido)-phenylamino)quinazolin-6-yl)-3-morpholinopropanamide-TFA (**3i**). Compound **3i** was prepared as described in the general procedure using DCM (3 mL), 3-morpholinopropanoic acid (50 mg, 256 μ mol), (COCl)₂ (22.4 μ L, 256 μ mol), DMF (three drops), and **3e** (50 mg, 68.5 μ mol) in 2 mL of NMP. Treatment of the crude with a solution of 25% morpholine in THF (2.5 mL) for 30 min led to Fmoc-deprotection. After evaporation of the volatiles under reduced pressure, the crude product was purified by preparative HPLC (H₂O/MeCN + 0.1% TFA) yielding 37 mg (48.5 μ mol, 71%) of the desired product as a yellow solid: ¹H NMR (400 MHz, DMSO-*d*₆) δ 11.56 (s, 1H), 10.92 (s, 1H), 9.52 (s, 1H), 8.98 (s, 1H), 8.85 (s, 2H), 8.08 (dd, *J* = 9.1, 1.5 Hz, 1H), 7.90 (d, *J* = 9.0 Hz, 1H), 7.55 (q, *J* = 9.3 Hz, 5H), 7.44 (t, *J* = 8.0 Hz, 2H), 7.27 (d, *J* = 4.7 Hz, 2H), 7.07 (d, *J* = 7.9 Hz, 1H), 6.38 (s, 1H), 4.01 (d, *J* = 11.2 Hz, 2H), 3.69 (t, *J* = 11.1 Hz, 2H), 3.49 (t, *J* = 7.2 Hz, 4H), 3.17 (d, *J* = 9.7 Hz, 2H), 2.99 (t, *J* = 7.2 Hz, 2H), 1.29 (s, 9H); ¹³C NMR (101 MHz, DMSO-*d*₆) δ 168.35, 161.03, 159.37, 159.19, 158.83, 158.47, 158.11, 151.93, 149.72, 139.55, 138.72, 138.28, 137.30, 134.56, 130.69, 130.20, 129.33, 125.57, 120.55, 118.19, 118.09, 117.32, 115.28, 114.41, 113.98, 112.90, 96.55, 63.43, 51.85, 51.45, 32.14, 30.21. HRMS (ESI-MS) calcd: 649.33576 for C₃₅H₄₁N₁₀O₃ [M + H⁺]. Found: 649.33563.

General Procedure for the Preparation of Aminophenyl-3-(3-*tert*-butyl-1-(3-nitrophenyl)-1H-pyrazol-5-yl)urea Hydrochlorides (13**, **14**).** The corresponding *N*-Boc-protected molecules **9** and **10** were treated with 4 M HCl in dioxane for about 45 min at room temperature. The volatiles were removed in vacuo, giving the desired product, which was further used without further purification.

1-(4-Aminophenyl)-3-(3-*tert*-butyl-1-(3-nitrophenyl)-1H-pyrazol-5-yl)urea Hydrochloride (13**).** Compound **13** was prepared as described in the general procedure using **9** (100 mg, 200 μ mol) and 4 M HCl in dioxane (3 mL) to obtain 85 mg (197 μ mol, 99%) of a fawn solid: ¹H NMR (400 MHz, DMSO-*d*₆) δ 10.21 (s, 2H), 9.86 (s, 1H), 9.16 (s, 1H), 8.36 (s, 1H), 8.20 (d, *J* = 8.1 Hz, 1H), 8.07 (d, *J* = 8.1 Hz, 1H), 7.80–7.76 (m, 1H), 7.50 (d, *J* = 8.8 Hz, 2H), 7.29 (d, *J* = 8.7 Hz, 2H), 6.41 (s, 1H), 1.30 (s, 9H); ¹³C NMR (101 MHz, DMSO-*d*₆) δ 161.93, 152.27, 148.12, 139.56, 139.38, 137.54, 130.81, 129.44, 125.21, 123.84, 121.38, 118.88, 117.86, 98.24, 32.20, 30.05. HRMS (ESI-MS) calcd: 395.18262 for C₂₀H₂₃N₆O₃ [M + H⁺]. Found: 395.18221.

1-(3-Aminophenyl)-3-(3-*tert*-butyl-1-(3-nitrophenyl)-1H-pyrazol-5-yl)urea Hydrochloride (14**).** Compound **14** was prepared as described in the general procedure using **10** (113 mg, 230 μ mol) and 4 M HCl in dioxane (5 mL) to obtain 98 mg (228 μ mol, 99%) of a fawn solid: ¹H NMR (400 MHz, DMSO-*d*₆) δ 10.27 (s, 2H), 10.00 (s, 1H), 9.19 (s, 1H), 8.36 (s, 1H), 8.20 (dd, *J* = 8.2, 1.3 Hz, 1H), 8.07 (dd, *J* = 8.1, 1.0 Hz, 1H), 7.78 (t, *J* = 8.2 Hz, 1H), 7.62 (s, 1H), 7.40–7.31 (m, 2H), 6.97 (dd, *J* = 6.5, 2.1 Hz, 1H), 6.41 (s, 1H), 1.30 (s, 9H); ¹³C NMR (101 MHz, DMSO-*d*₆) δ 161.97, 152.20, 148.15, 140.71, 139.58, 137.45, 132.05, 130.85, 130.17, 129.40, 121.41, 117.86, 117.43, 116.57, 112.52, 98.26, 32.22, 30.07. HRMS (ESI-MS) calcd: 395.18262 for C₂₀H₂₃N₆O₃ [M + H⁺]. Found: 395.18182.

4-Chloro-6-nitroquinazoline or 4-Chloroquinazoline. A two-neck flask was flushed with argon and charged with 6-nitroquinazolin-4-ol or quinazolin-4-ol and thionyl chloride. A catalytic amount of DMF was added, and the reaction mixture was refluxed at 80 °C overnight.

The thionyl chloride was evaporated under reduced pressure, and the remaining residue was dried under high vacuum and used without further purification.

1-(3-*tert*-Butyl-1-(3-nitrophenyl)-1H-pyrazol-5-yl)-3-(4-(6-nitroquinazolin-4-ylamino)phenyl)urea (3a**).** A solution of the amino hydrochloride **13** (77 mg, 179 μ mol) and DIPEA (153 μ L, 894 μ mol) in DCM (10 mL) was stirred for 5 min at room temperature. Then freshly prepared 4-chloro-6-nitroquinazoline (55 mg, 215 μ mol) was added, and the resulting reaction mixture was stirred for 23 h at room temperature. After addition of saturated sodium bicarbonate solution the aqueous layer was extracted with EtOAc (3 \times 10 mL) and the combined organic layers were dried over Na₂SO₄. The volatiles were removed in vacuo, and the purification of the crude on silica gel (1–4% MeOH/DCM) led to 45.1 mg (79.0 μ mol, 44%) of an orange solid: ¹H NMR (400 MHz, DMSO-*d*₆) δ 10.41 (s, 1H), 9.63 (s, 1H), 9.11 (s, 1H), 8.65 (s, 1H), 8.60 (s, 1H), 8.54 (dd, *J* = 9.2, 2.4 Hz, 1H), 8.39 (s, 1H), 8.23 (d, *J* = 8.1 Hz, 1H), 8.07 (d, *J* = 8.1 Hz, 1H), 7.90 (d, *J* = 9.1 Hz, 1H), 7.82 (t, *J* = 8.1 Hz, 1H), 7.70 (d, *J* = 8.7 Hz, 2H), 7.45 (d, *J* = 8.8 Hz, 2H), 6.43 (s, 1H), 1.31 (s, 9H); ¹³C NMR (101 MHz, DMSO-*d*₆) δ 161.99, 158.79, 157.89, 153.15, 152.16, 148.17, 144.48, 139.73, 137.79, 136.06, 132.81, 130.88, 129.58, 129.44, 126.61, 123.74, 121.46, 120.87, 118.59, 117.89, 98.20, 35.46, 32.25, 30.11. HRMS (ESI-MS) calcd: 568.20514 for C₂₈H₂₆N₉O₅ [M + H⁺]. Found: 568.20480.

General Procedure for the Preparation of 1,3- And 1,4-Fused Nitro-Substituted Hybrid Compounds (3b**, **4a**).** A suspension of **13** or **14** and freshly prepared 4-chloroquinazoline in 2-propanol was stirred for 3 h at 75 °C refluxing temperature. An excess of saturated sodium bicarbonate solution was added to the chilled reaction batch followed by extraction of the aqueous layer with EtOAc (4 \times 20 mL). The combined organic layers were dried over Na₂SO₄, and the solvent was removed under reduced pressure before the crude material was purified on silica gel.

1-(3-*tert*-Butyl-1-(3-nitrophenyl)-1H-pyrazol-5-yl)-3-(4-(quinazolin-4-ylamino)phenyl)urea (3b**).** Compound **3b** was prepared as described in the general procedure using **13** (137 mg, 0.32 mmol), 4-chloroquinazoline (116 mg, 0.70 mmol), and 2-propanol (6 mL). Silica gel column chromatography was performed using 2–4% MeOH/DCM and led to 80 mg (0.15 mmol, 47%) of the desired product as white solid: ¹H NMR (400 MHz, DMSO-*d*₆) δ 9.75 (s, 1H), 9.06 (s, 1H), 8.58 (s, 1H), 8.56–8.50 (m, 2H), 8.40 (t, *J* = 2.1 Hz, 1H), 8.23 (ddd, *J* = 8.3, 2.2, 0.7 Hz, 1H), 8.11–8.04 (m, 1H), 7.84 (dt, *J* = 14.9, 4.5 Hz, 2H), 7.77 (d, *J* = 8.0 Hz, 1H), 7.72 (d, *J* = 8.9 Hz, 2H), 7.66–7.59 (m, 1H), 7.43 (d, *J* = 8.9 Hz, 2H), 6.44 (s, 1H), 1.31 (s, 9H); ¹³C NMR (101 MHz, DMSO-*d*₆) δ 161.89, 157.73, 154.59, 152.07, 149.57, 148.12, 139.68, 137.80, 135.32, 133.59, 132.90, 130.81, 129.53, 127.73, 126.12, 123.28, 122.91, 121.37, 118.56, 117.85, 115.10, 98.02, 32.18, 30.06. HRMS (ESI-MS) calcd: 523.22006 for C₂₈H₂₇N₈O₃ [M + H⁺]. Found: 523.21936.

1-(3-*tert*-Butyl-1-(3-nitrophenyl)-1H-pyrazol-5-yl)-3-(3-(quinazolin-4-ylamino)phenyl)urea (4a**).** Compound **4a** was prepared as described in the general procedure using **14** (135 mg, 0.31 mmol), 4-chloroquinazoline (130 mg, 0.79 mmol), and 2-propanol (6 mL). Silica gel column chromatography was performed using 1–2% MeOH/DCM yielding 106 mg (0.20 mmol, 65%) of the desired product as light yellow solid: ¹H NMR (400 MHz, DMSO-*d*₆) δ 9.79 (s, 1H), 9.15 (s, 1H), 8.59 (t, *J* = 8.7 Hz, 3H), 8.39 (t, *J* = 2.0 Hz, 1H), 8.23 (dd, *J* = 8.2, 1.5 Hz, 1H), 8.07 (dd, *J* = 8.1, 1.1 Hz, 1H), 7.99 (s, 1H), 7.89–7.76 (m, 3H), 7.67–7.60 (m, 1H), 7.49 (d, *J* = 7.9 Hz, 1H), 7.31–7.20 (m, 2H), 6.44 (s, 1H), 1.30 (s, 9H); ¹³C NMR (101 MHz, DMSO-*d*₆) δ 161.92, 157.78, 154.42, 151.91, 149.62, 148.14, 139.64, 139.55, 139.41, 137.77, 133.04, 130.83, 129.57, 128.72, 127.77, 126.27, 123.08, 121.41, 117.95, 116.55, 115.19, 113.88, 112.44, 97.75, 32.19, 30.06. HRMS (ESI-MS) calcd: 523.22006 for C₂₈H₂₇N₈O₃ [M + H⁺]. Found: 523.21933.

1-(1-(3-Aminophenyl)-3-*tert*-butyl-1H-pyrazol-5-yl)-3-(4-(6-aminoquinazolin-4-ylamino)phenyl)urea (3c**).** A solution of **3a** (79 mg, 0.14 mmol) in EtOH (5 mL) was treated with ammonium formate (52 mg, 0.82 mmol) and 5% Pd on charcoal (29 mg, 14 μ mol) for 2 h at reflux. The catalyst/reaction mixture was filtered over Celite, and the filtrate was concentrated in vacuo. The crude material was purified on silica gel (4% MeOH/DCM) yielding 48.3 mg (0.1 mmol, 71%) of a yellow-orange solid: ¹H NMR (400 MHz, DMSO-*d*₆) δ 9.29 (s, 1H),

9.18 (s, 1H), 8.41 (s, 1H), 8.29 (s, 1H), 7.74 (d, $J = 8.9$ Hz, 2H), 7.51 (d, $J = 8.8$ Hz, 1H), 7.42 (d, $J = 8.9$ Hz, 2H), 7.36 (s, 1H), 7.23 (dd, $J = 8.8, 2.0$ Hz, 1H), 7.18–7.14 (m, 1H), 6.72 (s, 1H), 6.62 (d, $J = 8.1$ Hz, 2H), 6.37 (s, 1H), 5.55 (s, 2H), 5.42 (s, 2H), 1.28 (s, 9H); ^{13}C NMR (101 MHz, DMSO- d_6) δ 160.24, 156.07, 151.36, 150.04, 149.79, 147.15, 142.46, 139.11, 137.25, 134.82, 134.32, 129.57, 128.61, 123.44, 122.64, 118.18, 116.61, 112.97, 111.50, 110.02, 101.19, 93.67, 32.03, 30.31. HRMS (ESI-MS) calcd: 508.25678 for $\text{C}_{28}\text{H}_{30}\text{N}_9\text{O}$ $[\text{M} + \text{H}^+]$. Found: 508.25641.

General Procedure for the Preparation of 1,3- And 1,4-Fused Amino-Substituted Hybrid Compounds (3d, 4b). A suspension of **3b** or **4a** and SnCl_2 in EtOH was stirred for 1.5–3 h at 70 °C. The reaction mixture was concentrated in vacuo to the starting volume. Subsequently water was added, and the resulting solution was extracted with EtOAc (7×30 mL). The combined organic layers were dried over Na_2SO_4 , and the volatiles were removed under reduced pressure before the crude material was purified on silica gel.

1-(1-(3-Aminophenyl)-3-tert-butyl-1H-pyrazol-5-yl)-3-(4-(quinazolin-4-ylamino)phenyl)urea (3d). Compound **3d** was prepared as described in the general procedure using **3b** (84 mg, 0.16 mmol), SnCl_2 (61 mg, 0.32 mmol), and EtOH (7 mL). Silica gel column chromatography was performed (1–4% MeOH/DCM) resulting in 47 mg (0.10 mmol, 63%) of the desired product as a yellow solid: ^1H NMR (400 MHz, DMSO- d_6) δ 9.77 (s, 1H), 9.14 (s, 1H), 8.57–8.51 (m, 2H), 8.36 (s, 1H), 7.85 (t, $J = 7.6$ Hz, 1H), 7.77 (d, $J = 8.2$ Hz, 1H), 7.73 (d, $J = 8.9$ Hz, 2H), 7.65–7.59 (m, 1H), 7.45 (d, $J = 8.9$ Hz, 2H), 7.16 (t, $J = 7.9$ Hz, 1H), 6.69 (t, $J = 1.9$ Hz, 1H), 6.64–6.57 (m, 2H), 6.37 (s, 1H), 5.46 (s, 2H), 1.27 (s, 9H); ^{13}C NMR (101 MHz, DMSO- d_6) δ 160.20, 157.74, 154.57, 151.21, 149.79, 149.44, 139.05, 137.18, 135.57, 133.34, 132.95, 129.55, 127.63, 126.17, 123.37, 122.94, 118.12, 115.09, 112.95, 111.47, 110.01, 93.47, 32.00, 30.28. HRMS (ESI-MS) calcd: 493.24588 for $\text{C}_{28}\text{H}_{29}\text{N}_8\text{O}$ $[\text{M} + \text{H}^+]$. Found: 493.24541.

1-(1-(3-Aminophenyl)-3-tert-butyl-1H-pyrazol-5-yl)-3-(3-(quinazolin-4-ylamino)phenyl)urea (4b). Compound **4b** was prepared as described in the general procedure using **4a** (145 mg, 0.28 mmol), SnCl_2 (156 mg, 0.82 mmol), and EtOH (10 mL). Silica gel column chromatography was performed (1–4% MeOH/DCM) resulting in 82 mg (0.17 mmol, 61%) of the desired product as a white solid: ^1H NMR (400 MHz, DMSO- d_6) δ 9.80 (s, 1H), 9.21 (s, 1H), 8.61–8.57 (m, 2H), 8.39 (s, 1H), 8.03 (s, 1H), 7.87 (t, $J = 7.6$ Hz, 1H), 7.79 (d, $J = 8.1$ Hz, 1H), 7.64 (t, $J = 7.6$ Hz, 1H), 7.50 (d, $J = 7.8$ Hz, 1H), 7.29 (t, $J = 8.0$ Hz, 1H), 7.23 (d, $J = 8.3$ Hz, 1H), 7.16 (t, $J = 7.9$ Hz, 1H), 6.69 (t, $J = 1.9$ Hz, 1H), 6.63–6.58 (m, 2H), 6.37 (s, 1H), 5.45 (s, 2H), 1.26 (s, 9H); ^{13}C NMR (101 MHz, DMSO- d_6) δ 160.21, 157.78, 154.42, 151.10, 149.80, 149.60, 139.59, 139.57, 139.02, 137.13, 133.05, 129.58, 128.75, 127.75, 126.27, 123.09, 116.29, 115.20, 113.52, 112.97, 112.05, 111.50, 110.02, 93.34, 31.99, 30.27. HRMS (ESI-MS) calcd: 493.24588 for $\text{C}_{28}\text{H}_{29}\text{N}_8\text{O}$ $[\text{M} + \text{H}^+]$. Found: 493.24543.

Protein Preparations. Protein preparations of cSrc and cSrc T338M were expressed and purified as described elsewhere.³⁰ DNA encoding wild-type human Abl (residues S229–Q513; isoform 1a numbering) in a pET28a vector with an N-terminal His₆-tag followed by a thrombin cleavage site was purchased from GeneArt, Regensburg, Germany. Abl protein was coexpressed with YopH (Yersinia outer protein H) in *Escherichia coli* BL21-DE3 as described elsewhere.⁴⁰ After harvest and cell lysis, Abl protein was enriched by Ni-NTA chromatography, followed by gel filtration (High Load 16/60 Superdex 75, GE Healthcare) for buffer exchange (50 mM Tris, 150 mM NaCl, 2.5 mM CaCl_2 , 0.1% v/v 2-mercaptoethanol, pH 8.0). Eluate containing Abl protein was collected and the His-tag was removed by digestion with thrombin (GE Healthcare) at 4 °C overnight. Cleaved protein was isolated by ion exchange chromatography (MonoQ 5/50 GL; GE Healthcare) using buffers A (50 mM Tris, 1 mM DTT, 5% v/v glycerol, pH 8.5) and B (buffer A + 1 M NaCl) (0–30% B over 20 min; 1 mL/min). Finally, the buffer was adjusted to 25 mM Tris, 75 mM NaCl, 10% v/v glycerol, 5 mM DTT, pH 7.3, by gel filtration, and the protein was flash-frozen in small aliquots. All purification steps were carried out at 4 °C. Correct mass was confirmed by ESI-MS. Abl T315I was purchased from invitrogen (Lot no. 39639B, PV3866). KIT wild-type and KIT

V559D/T670I were purchased from Proqinase (Lot no. 010, 0997-0000-1 and Lot no. 002, 1044-0000-1).

Activity Based Assay for IC₅₀ Determination. IC₅₀ determinations for cSrc, Abl, and KIT kinases were measured with the KinEASE-TK assay from Cisbio according to the manufacturer's instructions. A biotinylated poly-Glu-Tyr substrate peptide was phosphorylated by the specific kinase of interest. After completion of the reaction, an anti-phosphotyrosine antibody labeled with europium cryptate and streptavidin labeled with the fluorophore XL665 were added. FRET between europium cryptate and XL665 was measured to quantify the phosphorylation of the substrate peptide. ATP concentrations were set at their respective K_M values (15 μM for wild-type cSrc, 1 μM for cSrc-T338M, 30 μM for wild-type Abl, 6 μM for Abl T315I, 90 μM for wild-type KIT and 20 μM for KIT V559D/T670I). A concentration of 100 nM substrate was used for wild-type and drug-resistant cSrc as well as Abl, while 250 nM was used for Abl T315I and 350 or 300 nM was used for KIT wild-type and KIT V559D/T670I respectively. Kinase and inhibitor were preincubated for 30–60 min before the reaction was started by addition of ATP and substrate peptide. A Tecan Safire² or Infinite M1000 plate reader was used to measure the fluorescence of the samples at 620 nm (Eu-labeled antibody) and 665 nm (XL665 labeled streptavidin) 60 μs after excitation at 317 nm. The quotient of both intensities for reactions made with eight different inhibitor concentrations was fit to a Hill four-parameter equation to determine IC₅₀ values. Each reaction was performed in duplicate, and at least three independent determinations of each IC₅₀ were made.

Crystallization and Structure Determination of cSrc-3g and cSrc-3h. For all complex structures, 2500 μM inhibitor (prepared in DMSO) was preincubated along with 250 μM wild-type cSrc (stored in 20 mM Tris pH 8.0, 100 mM NaCl, 1 mM DTT) for 1 h on ice to form the enzyme–inhibitor complex prior to crystallization. In the case of both **3g** and **3h**, crystals were grown using the hanging drop method at 20 °C after mixing 1–1.5 μL of protein–inhibitor solution with 1 μL of reservoir solution (125 mM MES (pH 6–7), 9–11.5% PEG 20000, 5% (v/v) glycerol). All crystals were directly frozen without the addition of glycerol. Diffraction data of the cSrc–**3g** complex crystal was measured in-house to a resolution of 3.30 Å (Bruker AXS microstar); the other data set was collected at the PX10SA beamline of the Swiss Light Source (PSI, Villigen, Switzerland) to a resolution of 2.7 Å for cSrc–**3h**, using wavelengths close to 1 Å. All data sets were processed with XDS⁴¹ and scaled using XSCALE.⁴¹

Structure Determination and Refinement of cSrc–3g and cSrc–3h. All cSrc–inhibitor complex structures were solved by molecular replacement with PHASER⁴² using the published cSrc structure 2OIQ⁴³ as template. The two cSrc molecules in the asymmetric unit were manually modified using the program COOT.⁴⁴ The model was first refined with CNS⁴⁵ using simulated annealing to remove model bias. The final refinement was performed with REFMACS.⁴⁶ Inhibitor topology files were generated using the Dundee PRODRG2 server.⁴⁷ Refined structures were validated with PROCHECK.⁴⁸ Data collection, structure refinement statistics, PDB-ID codes, and further details for the data collection, as well as Ramachandran plot results, are shown in Table S1, Supporting Information. PyMOL⁴⁹ was used to generate the figures.

Reagents and Antibodies. Imatinib, sunitinib, dovitinib, and ponatinib were purchased from LC Laboratories (Woburn, MA). Rabbit polyclonal antibodies to KIT and phospho-KIT Y703 were from DAKO (Carpinteria, CA) and Cell Signaling (Beverly Hills, CA), respectively. Polyclonal rabbit antibodies to total p42/44 mitogen-activated protein kinase (MAPK), phospho-p44/42 MAPK T202/Y204, phospho-AKT S473, total AKT, were from Cell Signaling (Beverly, MA). Beta Actin antibodies were purchased from Sigma (St. Louis, MO).

Cellular Studies. GIST-T1, GIST-T1 T670I, and GIST-48B cell lines were cultured as previously described.⁵⁰ Viability studies were carried out using a sulforhodamin (SRB) assay.⁵¹ For these studies, the cell lines were plated at 15 000 to 30 000 cells per well in a 96-well flat-bottom plate (Falcon, Lincoln, NJ), cultured in serum-containing media for 1 day, and then incubated for 72 h with KIT inhibitors and

DMSO-only solvent control. The SRB assay absorption was measured with a Genion luminometer (Tecan, Crailsheim, Germany), and the data were normalized to the DMSO-only control group. All experimental points were measured in triplicate wells for each plate and were replicated in at least two plates.

Western Blotting. Protein lysates were prepared from cell line monolayers according to standard protocols.⁵² Protein concentrations were determined with the Bio-Rad Protein Assay (Bio-Rad Laboratories, Hercules, CA). Electrophoresis and immunoblotting were carried out as previously described.⁵³ Changes in protein expression and phosphorylation as visualized by chemiluminescence were captured and quantified using a FUJI LAS3000 system with Science Lab 2001 ImageGauge 4.0 software (Fujifilm Medical Systems, Stamford CT, USA).

GIST Cell Lines. GIST-T1 was established from a human, untreated, metastatic GIST containing a 57 bp deletion in *KIT* exon 11, which is highly sensitive to imatinib at low nanomolar doses.³⁵ GIST-T1 harbors a homozygous deletion and is p53 negative as measured by qRT-PCR and Western blot analysis. GIST-48 was established from a GIST that had progressed, after initial clinical response, during imatinib therapy. GIST-48 has a primary, homozygous *KIT* exon 11 missense mutation (V560D) and a heterozygous secondary *KIT* exon 17 (kinase activation loop) mutation (D820A).⁵⁴ GIST-48 is imatinib-resistant, due to a secondary *KIT* exon 17 mutation. GIST-48B is a subline of GIST-48, which, despite retaining the activating *KIT* mutation in all cells, expresses *KIT* transcript (data not shown) and protein at essentially undetectable levels.⁵⁵ GIST-48B is *TP53* wild-type and expresses p53 RNA and protein as measured by qRT-PCR and Western blot analysis. GIST-48 and GIST-48B cell lines have been established at the Brigham and Women's Hospital in Boston, USA, by the Group of Professor Jonathan A. Fletcher. GIST-T1 has been established by Takahiro Taguchi at the Kochi University in Japan. GIST-T1 T670I was generated and kindly provided by Prof. Brian Rubin, Department of Molecular Genetics, Lerner Research Institute and Department of Anatomic Pathology and Taussing Cancer Center, Cleveland Clinic, Cleveland, OH 44195.

■ ASSOCIATED CONTENT

■ Supporting Information

Detailed synthetic procedures for the preparation of **6a** and **6b** as well as synthetic schemes for **3c,d**, **4b**, and **6a,b**, crystal X-ray structure data of **3g** and **3h** in complex with cSrc, modeling studies of **3g** into the catalytic domains of Abl T315I and KIT T670I, selectivity profiling data of **3d**, CYP inhibition data, cytotoxicity data, Ba/F3 Bcr-Abl (and T315I) proliferation assay data, and a detailed overview of **3h**–cSrc interactions including electron density information. This material is available free of charge via the Internet at <http://pubs.acs.org>.

Accession Codes

PDB ID codes 3TZ7 and 3TZ8.

■ AUTHOR INFORMATION

Corresponding Authors

*PD Dr. Sebastian Bauer: phone +49 (0)201-723 85558, fax +49 (0)201-723 5547; e-mail sebastian.bauer@uk-essen.de.

*Prof. Dr. Daniel Rauh: phone +49 (0)231-755 7056, fax +49 (0)231-755 5159, e-mail daniel.rauh@tu-dortmund.de.

Present Addresses

M.L.S.: Howard Hughes Medical Institute, Department of Cellular and Molecular Pharmacology, University of California, San Francisco, California 94158, USA.

J.M.H. and S.H.: Blackfield AG, Gottfried-Hagen-Str. 60, 51105 Cologne, Germany.

Notes

The authors declare the following competing financial interest(s): RKT is a founder and shareholder of Blackfield AG, a company focused on cancer genome diagnostics and

cancer genomics-based drug discovery. RKT received consulting and lecture fees (Sanofi-Aventis, Merck, Roche, Lilly, Boehringer Ingelheim, Astra-Zeneca, Atlas-Biolabs, Daiichi-Sankyo, Blackfield AG) as well as research support (Merck, EOS and AstraZeneca). DR received consultant and lecture fees from Astra-Zeneca, Merck-Serono, Takeda, Pfizer, Boehringer Ingelheim and Sanofi-Aventis.

■ ACKNOWLEDGMENTS

We thank Brian Rubin for kindly providing GIST-T1 T670I and Idoia Lahortiga for providing Ba/F3 cells. We thank Jonathan A. Fletcher for providing the GIST48B and T. Taguchi for providing the GIST T1. This work was cofunded by the German federal state North Rhine Westphalia (NRW) and the European Union (European Regional Development Fund: Investing In Your Future), the German Federal Ministry for Education and Research (NGFNPlus) (Grant Nos. BMBF 01GS08104 and 01GS08100), the EU-Framework Programme CURELUNG (HEALTH-F2-2010-258677), the Deutsche Forschungsgemeinschaft through TH1386/3-1 and through SFB832, the Max Planck Society, the Behrens-Weise Foundation (M.I.F.A.NEUR8061), Stand Up To Cancer–American Association for Cancer Research Innovative Research Grant (No. SU2C-AACR-IR60109), and an anonymous foundation. This work was furthermore supported by funding from Max-Eder Fellowship from the Deutsche Krebshilfe (S. Bauer) and the Life Raft Group Research Initiative (S. Bauer). M.L.S. is a fellow of the International Association for the Study of Lung Cancer (IASLC).

■ ABBREVIATIONS

Abl Abelson kinase; Akt protein kinase B; Bcr breakpoint cluster region; cSrc cellular sarcoma kinase; CYP cytochrome P450; GIST gastrointestinal stromal tumors; KIT mast/stem cell growth factor receptor kinase; LMS leiomyosarcoma; LPS liposarcoma; MPNST malignant peripheral nerve sheath tumor; GI₅₀ concentration for 50% of maximal inhibition of cell proliferation; IC₅₀ concentration causing 50% inhibition of enzyme activity; DMSO dimethyl sulfoxide; DIPEA *N,N*-diisopropylethylamine; DCM dichloromethane; THF tetrahydrofuran; DMF dimethylformamide; NMP *N*-methylpyrrolidinone; MES 2-(*N*-morpholino)ethanesulfonic acid; PEG poly(ethylene glycol)

■ REFERENCES

- (1) Rabiller, M.; Getlik, M.; Klüter, S.; Richters, A.; Tückmantel, S.; Simard, J. R.; Rauh, D. Proteus in the world of proteins: Conformational changes in protein kinases. *Arch. Pharm. (Weinheim, Ger.)* **2010**, *343*, 193–206.
- (2) Gschwind, A.; Fischer, O. M.; Ullrich, A. The discovery of receptor tyrosine kinases: targets for cancer therapy. *Nat. Rev. Cancer* **2004**, *4*, 361–370.
- (3) Sordella, R.; Bell, D. W.; Haber, D. A.; Settleman, J. Gefitinib-sensitizing EGFR mutations in lung cancer activate anti-apoptotic pathways. *Science* **2004**, *305*, 1163–1167.
- (4) Weinstein, I. B.; Joe, A. K. Mechanisms of disease: Oncogene addiction—a rationale for molecular targeting in cancer therapy. *Nat. Clin. Pract. Oncol.* **2006**, *3*, 448–457.
- (5) Shah, N. P.; Tran, C.; Lee, F. Y.; Chen, P.; Norris, D.; Sawyers, C. L. Overriding imatinib resistance with a novel ABL kinase inhibitor. *Science* **2004**, *305*, 399–401.
- (6) Steinberg, M. Dasatinib: A tyrosine kinase inhibitor for the treatment of chronic myelogenous leukemia and philadelphia

chromosome-positive acute lymphoblastic leukemia. *Clin. Ther.* **2007**, *29*, 2289–2308.

(7) Paez, J. G.; Janne, P. A.; Lee, J. C.; Tracy, S.; Greulich, H.; Gabriel, S.; Herman, P.; Kaye, F. J.; Lindeman, N.; Boggon, T. J.; Naoki, K.; Sasaki, H.; Fujii, Y.; Eck, M. J.; Sellers, W. R.; Johnson, B. E.; Meyerson, M. EGFR mutations in lung cancer: Correlation with clinical response to gefitinib therapy. *Science* **2004**, *304*, 1497–1500.

(8) Balak, M. N.; Gong, Y.; Riely, G. J.; Somwar, R.; Li, A. R.; Zakowski, M. F.; Chiang, A.; Yang, G.; Ouerfelli, O.; Kris, M. G.; Ladanyi, M.; Miller, V. A.; Pao, W. Novel D761Y and common secondary T790M mutations in epidermal growth factor receptor-mutant lung adenocarcinomas with acquired resistance to kinase inhibitors. *Clin. Cancer Res.* **2006**, *12*, 6494–6501.

(9) Gajwala, K. S.; Wu, J. C.; Christensen, J.; Deshmukh, G. D.; Diehl, W.; DiNitto, J. P.; English, J. M.; Greig, M. J.; He, Y. A.; Jacques, S. L.; Lunney, E. A.; McTigue, M.; Molina, D.; Quenzer, T.; Wells, P. A.; Yu, X.; Zhang, Y.; Zou, A.; Emmett, M. R.; Marshall, A. G.; Zhang, H. M.; Demetri, G. D. KIT kinase mutants show unique mechanisms of drug resistance to imatinib and sunitinib in gastrointestinal stromal tumor patients. *Proc. Natl. Acad. Sci. U. S. A.* **2009**, *106*, 1542–1547.

(10) Heinrich, M. C.; Corless, C. L.; Demetri, G. D.; Blanke, C. D.; von Mehren, M.; Joensuu, H.; McGreevey, L. S.; Chen, C. J.; Van den Abbeele, A. D.; Druker, B. J.; Kiese, B.; Eisenberg, B.; Roberts, P. J.; Singer, S.; Fletcher, C. D.; Silberman, S.; Dimitrijevic, S.; Fletcher, J. A. Kinase mutations and imatinib response in patients with metastatic gastrointestinal stromal tumor. *J. Clin. Oncol.* **2003**, *21*, 4342–4349.

(11) Jabbour, E.; Cortes, J.; Kantarjian, H. Long-term outcomes in the second-line treatment of chronic myeloid leukemia: a review of tyrosine kinase inhibitors. *Cancer* **2011**, *117*, 897–906.

(12) Mok, T. S.; Wu, Y. L.; Thongprasert, S.; Yang, C. H.; Chu, D. T.; Saijo, N.; Sunpaweravong, P.; Han, B.; Margono, B.; Ichinose, Y.; Nishiwaki, Y.; Ohe, Y.; Yang, J. J.; Chewaskulyong, B.; Jiang, H.; Duffield, E. L.; Watkins, C. L.; Armour, A. A.; Fukuoka, M. Gefitinib or carboplatin-paclitaxel in pulmonary adenocarcinoma. *N. Engl. J. Med.* **2009**, *361*, 947–957.

(13) Druker, B. J.; Guilhot, F.; O'Brien, S. G.; Gathmann, I.; Kantarjian, H.; Gattermann, N.; Deininger, M. W.; Silver, R. T.; Goldman, J. M.; Stone, R. M.; Cervantes, F.; Hochhaus, A.; Powell, B. L.; Gabrilove, J. L.; Rousselot, P.; Reiffers, J.; Cornelissen, J. J.; Hughes, T.; Agis, H.; Fischer, T.; Verhoef, G.; Shepherd, J.; Saglio, G.; Gratwohl, A.; Nielsen, J. L.; Radich, J. P.; Simonsson, B.; Taylor, K.; Baccarani, M.; So, C.; Letvak, L.; Larson, R. A. Five-year follow-up of patients receiving imatinib for chronic myeloid leukemia. *N. Engl. J. Med.* **2006**, *355*, 2408–2417.

(14) Shah, N. P.; Nicoll, J. M.; Nagar, B.; Gorre, M. E.; Paquette, R. L.; Kuriyan, J.; Sawyers, C. L. Multiple BCR-ABL kinase domain mutations confer polyclonal resistance to the tyrosine kinase inhibitor imatinib (STI571) in chronic phase and blast crisis chronic myeloid leukemia. *Cancer Cell* **2002**, *2*, 117–125.

(15) Griswold, I. J.; MacPartlin, M.; Bumm, T.; Goss, V. L.; O'Hare, T.; Lee, K. A.; Corbin, A. S.; Stoffregen, E. P.; Smith, C.; Johnson, K.; Moseson, E. M.; Wood, L. J.; Polakiewicz, R. D.; Druker, B. J.; Deininger, M. W. Kinase domain mutants of Bcr-Abl exhibit altered transformation potency, kinase activity, and substrate utilization, irrespective of sensitivity to imatinib. *Mol. Cell. Biol.* **2006**, *26*, 6082–6093.

(16) Shah, N. P.; Sawyers, C. L. Mechanisms of resistance to STI571 in Philadelphia chromosome-associated leukemias. *Oncogene* **2003**, *22*, 7389–7395.

(17) Willis, S. G.; Lange, T.; Demehri, S.; Otto, S.; Crossman, L.; Niederwieser, D.; Stoffregen, E. P.; McWeeney, S.; Kovacs, I.; Park, B.; Druker, B. J.; Deininger, M. W. High-sensitivity detection of BCR-ABL kinase domain mutations in imatinib-naïve patients: correlation with clonal cytogenetic evolution but not response to therapy. *Blood* **2005**, *106*, 2128–2137.

(18) Sos, M. L.; Rode, H. B.; Heynck, S.; Peifer, M.; Fischer, F.; Kluter, S.; Pawar, V. G.; Reuter, C.; Heuckmann, J. M.; Weiss, J.; Ruddigkeit, L.; Rabiller, M.; Koker, M.; Simard, J. R.; Getlik, M.; Yuza, Y.; Chen, T. H.; Greulich, H.; Thomas, R. K.; Rauh, D. Chemo-

genomic profiling provides insights into the limited activity of irreversible EGFR Inhibitors in tumor cells expressing the T790M EGFR resistance mutation. *Cancer Res.* **2010**, *70*, 868–874.

(19) Heuckmann, J. M.; Rauh, D.; Thomas, R. K. Epidermal growth factor receptor (EGFR) signaling and covalent EGFR inhibition in lung cancer. *J. Clin. Oncol.* **2012**, *30*, 3417–3420.

(20) Wang, W. L.; Conley, A.; Reynoso, D.; Nolden, L.; Lazar, A. J.; George, S.; Trent, J. C. Mechanisms of resistance to imatinib and sunitinib in gastrointestinal stromal tumor. *Cancer Chemother. Pharmacol.* **2010**, *67* (Suppl 1), S15–S24.

(21) Antonescu, C. R. The GIST paradigm: Lessons for other kinase-driven cancers. *J. Pathol.* **2011**, *223*, 251–261.

(22) Gibbons, D. L.; Prich, S.; Kantarjian, H.; Cortes, J.; Quintas-Cardama, A. The rise and fall of gatekeeper mutations? The BCR-ABL1 T315I paradigm. *Cancer* **2011**, *118*, 293–299.

(23) Eide, C. A.; Adrian, L. T.; Tyner, J. W.; Mac Partlin, M.; Anderson, D. J.; Wise, S. C.; Smith, B. D.; Petillo, P. A.; Flynn, D. L.; Deininger, M. W.; O'Hare, T.; Druker, B. J. The ABL switch control inhibitor DCC-2036 is active against the chronic myeloid leukemia mutant BCR-ABL1T315I and exhibits a narrow resistance profile. *Cancer Res.* **2011**, *71*, 3189–3195.

(24) U.S. National Library of Medicine. <http://www.clinicaltrials.gov/>

(25) U.S. Food and Drug Administration. <http://www.fda.gov/>

(26) Fang, Z.; Grütter, C.; Rauh, D. Strategies for the selective regulation of kinases with allosteric modulators: exploiting exclusive structural features. *ACS Chem. Biol.* **2013**, *8*, 58–70.

(27) Backes, A. C.; Zech, B.; Felber, B.; Klebl, B.; Müller, G. Small-molecule inhibitors binding to protein kinase. Part II: The novel pharmacophore approach of type II and type III inhibition. *Expert Opin. Drug Discovery* **2008**, *3*, 1427–1449.

(28) Janne, P. A.; Gray, N.; Settleman, J. Factors underlying sensitivity of cancers to small-molecule kinase inhibitors. *Nat. Rev. Drug Discovery* **2009**, *8*, 709–723.

(29) Liu, Y.; Gray, N. S. Rational design of inhibitors that bind to inactive kinase conformations. *Nat. Chem. Biol.* **2006**, *2*, 358–364.

(30) Getlik, M.; Grütter, C.; Simard, J. R.; Klüter, S.; Rabiller, M.; Rode, H. B.; Robubi, A.; Rauh, D. Hybrid compound design to overcome the gatekeeper T338M mutation in cSrc. *J. Med. Chem.* **2009**, *52*, 3915–3926.

(31) Hunter, C. A.; Singh, J.; Thornton, J. M. Pi-pi interactions: The geometry and energetics of phenylalanine-phenylalanine interactions in proteins. *J. Mol. Biol.* **1991**, *218*, 837–846.

(32) Wilhelm, S.; Carter, C.; Lynch, M.; Lowinger, T.; Dumas, J.; Smith, R. A.; Schwartz, B.; Simantov, R.; Kelley, S. Discovery and development of sorafenib: A multikinase inhibitor for treating cancer. *Nat. Rev. Drug Discovery* **2006**, *5*, 835–844.

(33) Barker, A. J.; Gibson, K. H.; Grundy, W.; Godfrey, A. A.; Barlow, J. J.; Healy, M. P.; Woodburn, J. R.; Ashton, S. E.; Curry, B. J.; Scarlett, L.; Henthorn, L.; Richards, L. Studies leading to the identification of ZD1839 (IRESSA): an orally active, selective epidermal growth factor receptor tyrosine kinase inhibitor targeted to the treatment of cancer. *Bioorg. Med. Chem. Lett.* **2001**, *11*, 1911–1914.

(34) Druker, B. J.; Tamura, S.; Buchdunger, E.; Ohno, S.; Segal, G. M.; Fanning, S.; Zimmermann, J.; Lydon, N. B. Effects of a selective inhibitor of the Abl tyrosine kinase on the growth of Bcr-Abl positive cells. *Nat. Med.* **1996**, *2*, 561–566.

(35) Nakatani, H.; Kobayashi, M.; Jin, T.; Taguchi, T.; Sugimoto, T.; Nakano, T.; Hamada, S.; Araki, K. STI571 (Gleevec) inhibits the interaction between c-KIT and heat shock protein 90 of the gastrointestinal stromal tumor cell line, GIST-T1. *Cancer Sci.* **2005**, *96*, 116–119.

(36) Copeland, R. A. Conformational adaptation in drug-target interactions and residence time. *Future Med. Chem.* **2011**, *3*, 1491–1501.

(37) Klebe, G. *Wirkstoffdesign: Entwurf und Wirkung von Arzneistoffen*. 2nd ed.; Spektrum Akademischer Verlag: Heidelberg, Germany, 2009.

(38) O'Hare, T.; Shakespeare, W. C.; Zhu, X.; Eide, C. A.; Rivera, V. M.; Wang, F.; Adrian, L. T.; Zhou, T.; Huang, W. S.; Xu, Q.; Metcalf,

C. A., 3rd; Tyner, J. W.; Loriaux, M. M.; Corbin, A. S.; Wardwell, S.; Ning, Y.; Keats, J. A.; Wang, Y.; Sundaramoorthi, R.; Thomas, M.; Zhou, D.; Snodgrass, J.; Commodore, L.; Sawyer, T. K.; Dalgarno, D. C.; Deininger, M. W.; Druker, B. J.; Clackson, T. AP24534, a pan-BCR-ABL inhibitor for chronic myeloid leukemia, potently inhibits the T315I mutant and overcomes mutation-based resistance. *Cancer Cell* **2009**, *16*, 401–412.

(39) Lozzio, C. B.; Lozzio, B. B. Human chronic myelogenous leukemia cell-line with positive Philadelphia chromosome. *Blood* **1975**, *45*, 321–334.

(40) Schneider, R.; Becker, C.; Simard, J. R.; Getlik, M.; Bohlke, N.; Janning, P.; Rauh, D. direct binding assay for the detection of type IV allosteric inhibitors of Abl. *J. Am. Chem. Soc.* **2012**, *134*, 9138–9141.

(41) Kabsch, W. Automatic processing of rotation diffraction data from crystals of initially unknown symmetry and cell constants. *J. Appl. Crystallogr.* **1993**, *26*, 795–800.

(42) Read, R. J. Pushing the boundaries of molecular replacement with maximum likelihood. *Acta Crystallogr., Sect. D: Biol. Crystallogr.* **2001**, *57*, 1373–1382.

(43) Seeliger, M. A.; Nagar, B.; Frank, F.; Cao, X.; Henderson, M. N.; Kuriyan, J. c-Src binds to the cancer drug imatinib with an inactive Abl/c-Kit conformation and a distributed thermodynamic penalty. *Structure* **2007**, *15*, 299–311.

(44) Emsley, P.; Cowtan, K. Coot: Model-building tools for molecular graphics. *Acta Crystallogr., Sect. D: Biol. Crystallogr.* **2004**, *60*, 2126–2132.

(45) Brünger, A. T.; Adams, P. D.; Clore, G. M.; DeLano, W. L.; Gros, P.; Grosse-Kunstleve, R. W.; Jiang, J. S.; Kuszewski, J.; Nilges, M.; Pannu, N. S.; Read, R. J.; Rice, L. M.; Simonson, T.; Warren, G. L. Crystallography & NMR system: A new software suite for macromolecular structure determination. *Acta Crystallogr., Sect. D: Biol. Crystallogr.* **1998**, *54*, 905–921.

(46) Murshudov, G. N.; Vagin, A. A.; Dodson, E. J. Refinement of macromolecular structures by the maximum-likelihood method. *Acta Crystallogr., Sect. D: Biol. Crystallogr.* **1997**, *53*, 240–255.

(47) Schüttelkopf, A. W.; van Aalten, D. M. PRODRG: A tool for high-throughput crystallography of protein-ligand complexes. *Acta Crystallogr., Sect. D: Biol. Crystallogr.* **2004**, *60*, 1355–1363.

(48) Laskowski, R. A.; MacArthur, M. W.; Moss, D. S.; Thornton, J. M. PROCHECK: A program to check the stereochemical quality of protein structures. *J. Appl. Crystallogr.* **1993**, *26*, 283–291.

(49) DeLano, W. L. The PyMOL Molecular Graphics System. <http://www.pymol.org>, 2002.

(50) Henze, J.; Mühlberg, T.; Simon, S.; Grabellus, F.; Rubin, B.; Taeger, G.; Schuler, M.; Treckmann, J.; Debiec-Rychter, M.; Taguchi, T.; Fletcher, J. A.; Bauer, S. p53 modulation as a therapeutic strategy in gastrointestinal stromal tumors. *PLoS ONE* **2012**, *7*, No. e37776.

(51) Vichai, V.; Kirtikara, K. Sulforhodamine B colorimetric assay for cytotoxicity screening. *Nat. Protoc.* **2006**, *1*, 1112–1116.

(52) Duensing, A.; Medeiros, F.; McConarty, B.; Joseph, N. E.; Panigrahy, D.; Singer, S.; Fletcher, C. D.; Demetri, G. D.; Fletcher, J. A. Mechanisms of oncogenic KIT signal transduction in primary gastrointestinal stromal tumors (GISTs). *Oncogene* **2004**, *23*, 3999–4006.

(53) Rubin, B. P.; Singer, S.; Tsao, C.; Duensing, A.; Lux, M. L.; Ruiz, R.; Hibbard, M. K.; Chen, C. J.; Xiao, S.; Tuveson, D. A.; Demetri, G. D.; Fletcher, C. D.; Fletcher, J. A. KIT activation is a ubiquitous feature of gastrointestinal stromal tumors. *Cancer Res.* **2001**, *61*, 8118–8121.

(54) Bauer, S.; Yu, L. K.; Demetri, G. D.; Fletcher, J. A. Heat shock protein 90 inhibition in imatinib-resistant gastrointestinal stromal tumor. *Cancer Res.* **2006**, *66*, 9153–9161.

(55) Mühlberg, T.; Zhang, Y.; Wagner, A. J.; Grabellus, F.; Bradner, J.; Taeger, G.; Lang, H.; Taguchi, T.; Schuler, M.; Fletcher, J. A.; Bauer, S. Inhibitors of deacetylases suppress oncogenic KIT signaling, acetylate HSP90, and induce apoptosis in gastrointestinal stromal tumors. *Cancer Res.* **2009**, *69*, 6941–6950.